Theory of de Haas-van Alphen Effect in Type-II Superconductors

Kouji Yasui and Takafumi Kita*
Division of Physics, Hokkaido University, Sapporo 060-0810, Japan
(Dated: February 6, 2008)

Theory of quasiparticle spectra and the de Haas-van Alphen (dHvA) oscillation in type-II superconductors are developed based on the Bogoliubov-de Gennes equations for vortex-lattice states. As the pair potential grows through the superconducting transition, each degenerate Landau level in the normal state splits into quasiparticle bands in the magnetic Brillouin zone. This brings Landau-level broadening, which in turn leads to the extra dHvA oscillation damping in the vortex state. We perform extensive numerical calculations for three-dimensional systems with various gap structures. It is thereby shown that (i) this Landau-level broadening is directly connected with the average gap at $H = 0$ along each Fermi-surface orbit perpendicular to the field $\mathbf{H}$; (ii) the extra dHvA oscillation attenuation is caused by the broadening around each extremal orbit. These results imply that the dHvA experiment can be a unique probe to detect band- and/or angle-dependent gap amplitudes. We derive an analytic expression for the extra damping based on the second-order perturbation with respect to the pair potential for the Luttinger-Ward thermodynamic potential. This formula reproduces all our numerical results excellently, and is used to estimate band-specific gap amplitudes from available data on $NbSe_2$, Nb_3Sn, and YNi_2B_2C. The obtained value for YNi_2B_2C is fairly different from the one through a specific-heat measurement, indicating presence of gap anisotropy in this material. C programs to solve the two-dimensional Bogoliubov-de Gennes equations are available at `http://phys.sci.hokudai.ac.jp/~kita/index-e.html`.

I. INTRODUCTION

The de Haas-van Alphen (dHvA) experiment on normal metals has been a unique and powerful tool to probe their Fermi surfaces.[1,2] The main purpose of this paper is to establish theoretically that it can even be used to detect detailed gap structures of type-II superconductors.

Back in 1976, Graebner and Robbins discovered the dHvA oscillation in 2H-$NbSe_2$ persisting down through the superconducting upper critical field H_{c2}.[3] It was after 15 years later when Ōnuki *et al.* first reconfirmed it.[4] Since then, however, a considerable number of materials have been found to display the dHvA oscillation in the vortex state. They include: $A15$ superconductors V_3Si[5,6] Nb_3Sn,[7] a borocarbide superconductor YNi_2B_2C,[8,9] heavy-fermion superconductors $CeRu_2$,[10] URu_2Si_2,[11,12] UPd_2Al_3,[13] $CeCoIn_5$,[14] and an organic superconductor κ-(BEDT-TTF)$_2$Cu(NCS)$_2$;[15] see Refs. 16 and 17 for a recent review. Basic features of the oscillation are be summarized as follows: (i) the dHvA frequencies remain unchanged through the transition; (ii) the oscillation amplitude experience an extra attenuation; (iii) the cyclotron mass does not change except for strongly correlated heavy fermion systems.

It is somewhat surprising that the dHvA oscillation is observable even in superconductors without a well-defined Fermi surface. Many theories have been presented to explain the persistent oscillation and the extra damping,[18,19,20,21,22,23,24,25,26,27,28,29,30] which may be classified into three categories.

The first approach applies a Bohr-Sommerfeld semiclassical quantization to either the Brandt-Pesch-Tewordt[31] (BPT) Green's function near H_{c2},[18] the electron number N at $H = 0$,[19] or Dyson's equation at $H = 0$,[20] for obtaining the oscillatory behavior of the magnetization. As may be seen by this diversity of the applications, however, there is no unique semiclassical quantization scheme for quasiparticles superconductors; thus, the validity of the procedure is not clear. This category includes Maki's theory,[18] which was later reproduced by Wasserman and Springford[21] by treating the BTP self-energy as the extra broadening factor in the normal-state thermodynamic potential and then following Dingle's procedure.[32] However, the BTP self-energy itself is obtained within the quasiclassical approximation without the Landau-level structure so that this approximation may also be questionable.

The second approach relies on some approximate analytic solutions for the Bogoliubov-de Gennes (BdG) equations or the equivalent Gor'kov equations, such as the coherent-potential approximation,[22,23] the diagonal-pairing approximation,[24] or the Ginzburg-Landau (GL) expansion for the free energy with respect to the order parameter.[25,26,27] However, quantitative estimations of those approximations are yet to be carried out. It should also be noted that the GL expansion necessarily integrates out the quasiparticle degrees of freedom, so that the physical origin of the extra oscillation damping may be obscured in the GL approach.

The third approach solves the BdG equations numerically without approximations.[29,30] Norman *et al.*[29] thereby extracted an analytic formula for the dHvA oscillation damping through a fitting to their numerical data.[29] However, it is a two-dimensional calculation for the isotropic s-wave pairing where the number of Landau levels below the Fermi level is $N_{\rm F} \sim 10$ at H_{c2}. As may be realized from the appearance of the quantized Hall effect, two-dimensional systems in high magnetic fields may be qualitatively different from three-dimensional systems. Thus, the obtained formula may

not be appropriate for describing real three-dimensional materials with $N_{\rm F} \gg 1$. On the other hand, another calculation by Miller and Györffy for a two-dimensional lattice model[30] corresponds to the low-field limit near H_{c1}[33] and may not be suitable to explain the experiments. Moreover, calculations for lattice models have a flaw that they cannot yield continuous magnetic oscillation due to the commensurability condition between the underlying lattice and the vortex lattice.

Notice finally that most of the above theories consider only the isotropic s-wave pairing. Especially, no numerical studies have been performed yet for anisotropic pairings or three-dimensional systems.

With these observations, we will perform both numerical and analytic calculations for three-dimensional BdG equations with various gap structures. They can be solved efficiently by the Landau-level-expansion method (LLX), which was formulated for vortex-lattice states of arbitrary pairing symmetry[34] and used successfully to compare low-energy quasiparticle spectra between s- and d-wave pairings.[35] We will thereby clarify how the discrete Landau levels experience quantitative changes as the pair potential grows below H_{c2}. Another purpose is to find out the connection between the gap anisotropy and the extra dHvA amplitude attenuation. Terashima *et al.*[9] reported a dHvA experiment on YNi_2B_2C where an oscillation is observed to persist down to a field $\sim 0.2H_{c2}$. On the other hand, a specific-heat experiment at $H=0$ shows a power-law behavior $\propto T^3$ at low temperatures,[36] indicating existence of gap anisotropy in this material. Indeed, Izawa *et al.*[37] recently reported presence of four point nodes in the gap based on a thermal-conductivity measurement. Miyake[19] argued that point or line nodes along the extremal orbit may weaken the damping, and proposed to use the dHvA effect as a probe for gap anisotropy. We examine this possibility in full details and present a quantitative theory on the issue.

This paper is organized as follows. Section II provides a formulation to solve the BdG equations for vortex-lattice states. Section III presents calculated quasiparticle spectra and the dHvA oscillation for two-dimensional systems to clarify their basic features as well as the origin of the extra dHvA oscillation damping in the vortex state. In Sec. IV, it is demonstrated that the gap anisotropy at $H=0$ can be detectable via the dHvA oscillation in the vortex state based on both numerical and analytic calculations for three-dimensional systems with various gap structures. Section V presents estimations of energy gap for $NbSe_2$, Nb_3Sn, and YNi_2B_2C using the analytic formula obtained in Appendix C. Section VI concludes the paper with a brief summary. In Appendix A, we derive a convenient expression for the thermodynamic potential. Appendix B summarizes the expressions of basis functions and overlap integrals used in the numerical calculations. In Appendix C, we derive an analytic expression for the extra dHvA oscillation damping in the vortex state. A brief report of the contents was already presented in Ref. 38.

II. FORMULATION

A. Bogoliubov-de Gennes equations

Throughout the paper we will rely on the mean-field BdG equations, which obtain the quasiparticle wavefunctions $\mathbf{u}_s$ and $\mathbf{v}_s^*$ with a positive eigenvalue $E_s > 0$ by

$$\int d\mathbf{r}_2 \begin{bmatrix} \underline{\mathcal{H}}(\mathbf{r}_1,\mathbf{r}_2) & \underline{\Delta}(\mathbf{r}_1,\mathbf{r}_2) \\ \underline{\Delta}^\dagger(\mathbf{r}_1,\mathbf{r}_2) & -\underline{\mathcal{H}}^*(\mathbf{r}_1,\mathbf{r}_2) \end{bmatrix} \begin{bmatrix} \mathbf{u}_s(\mathbf{r}_2) \\ -\mathbf{v}_s^*(\mathbf{r}_2) \end{bmatrix} = E_s \begin{bmatrix} \mathbf{u}_s(\mathbf{r}_1) \\ -\mathbf{v}_s^*(\mathbf{r}_1) \end{bmatrix} . \tag{1}$$

Here $\underline{\Delta}$ is the pair potential and $\underline{\mathcal{H}}$ denotes the normal-state Hamiltonian in the magnetic field; both are 2×2 matrices to describe the spin degrees of freedom. The symbol † denotes Hermitian conjugate in both the coordinate and spin variables as $[\underline{\Delta}^\dagger(\mathbf{r}_1,\mathbf{r}_2)]_{\sigma_1\sigma_2} = \Delta^*_{\sigma_2\sigma_1}(\mathbf{r}_2,\mathbf{r}_1)$ with $\sigma_j = \uparrow, \downarrow$. With this definition, we can see immediately that the matrix in Eq. (1) is Hermitian.

We adopt the free-particle Hamiltonian for $\underline{\mathcal{H}}$:

$$\underline{\mathcal{H}}(\mathbf{r}_1,\mathbf{r}_2) = \delta(\mathbf{r}_1-\mathbf{r}_2) \left\{ \frac{\left[-i\hbar\boldsymbol{\nabla}_2 + \frac{e}{c}\mathbf{A}(\mathbf{r}_2)\right]^2}{2m_{\rm e}} - \varepsilon_{\rm F} \right\} \underline{1} , \tag{2}$$

where $m_{\rm e}$, $-e$ ($e>0$), c, and $\varepsilon_{\rm F}$ are the electron mass, the electron charge, the light velocity, and the chemical potential, respectively. We will not consider the spin paramagnetism throughout. We also neglect the spatial variation of the magnetic field as appropriate for the relevant high-κ materials. Then, the vector potential $\mathbf{A}$ can be expressed using the symmetric gauge as

$$\mathbf{A}(\mathbf{r}) = -\frac{1}{2} B\hat{\mathbf{z}}\times\mathbf{r} , \tag{3}$$

where B denotes the average flux density, and we have chosen the field along $-\hat{\mathbf{z}}$ for convenience.

The pair potential in turn is given with respect to the quasiparticle wavefunctions as

$$\underline{\Delta}(\mathbf{r}_1,\mathbf{r}_2) = V(\mathbf{r}_1-\mathbf{r}_2)\, \underline{\Phi}(\mathbf{r}_1,\mathbf{r}_2) , \tag{4}$$

where V denotes the interaction and $\underline{\Phi}$ is the order parameter defined by

$$\underline{\Phi}(\mathbf{r}_1,\mathbf{r}_2) \equiv \sum_s \left[\mathbf{u}_s(\mathbf{r}_1)\mathbf{v}_s^{\rm T}(\mathbf{r}_2) - \mathbf{v}_s(\mathbf{r}_1)\mathbf{u}_s^{\rm T}(\mathbf{r}_2)\right] \times \frac{1}{2}\tanh\frac{E_s}{2k_{\rm B}T} , \tag{5}$$

with T the temperature and $^{\rm T}$ denoting the transpose.

It is shown in Appendix A that the thermodynamic potential corresponding to Eqs. (1)-(4) is given by

$$\Omega = -k_{\rm B}T\sum_s \ln(1+{\rm e}^{-E_s/k_{\rm B}T}) - \sum_s E_s \int |\mathbf{v}_s(\mathbf{r})|^2\, d\mathbf{r} - \frac{1}{2}\iint {\rm Tr}\, \underline{\Delta}^\dagger(\mathbf{r}_1,\mathbf{r}_2)\, \underline{\Phi}(\mathbf{r}_2,\mathbf{r}_1)\, {\rm d}\mathbf{r}_1 {\rm d}\mathbf{r}_2 , \tag{6}$$

where Tr denotes taking trace over spin variables. This expression will be useful to obtain an analytic expression for the extra dHvA amplitude attenuation in the vortex state. The magnetization is then calculated by

$$M = -\frac{\partial(\Omega/\mathcal{V})}{\partial B}\,, \tag{7}$$

where $\mathcal{V}$ is the volume of the system.

B. Vortex lattices and basic vectors

Solving the above equations for general non-uniform systems is a formidable task. For lattice states, however, it can be reduced into a numerically tractable problem using the symmetry that they are periodic with a single flux quantum $\phi_0 \equiv hc/2e$ per unit cell. We hence define a pair of basic vectors by

$$\begin{cases} \mathbf{a}_1 \equiv (a_{1x}, a_{1y}, 0) \\ \mathbf{a}_2 \equiv (0, a_2, 0) \end{cases}, \qquad (\mathbf{a}_1 \times \mathbf{a}_2)\cdot\hat{\mathbf{z}} = \frac{\phi_0}{B} = \pi l_B^2\,, \tag{8}$$

where $l_B \equiv \sqrt{\hbar c/eB}$ is the magnetic length. The basic vectors of the corresponding reciprocal lattice are then defined by

$$\begin{cases} \mathbf{b}_1 \equiv 2(\mathbf{a}_2 \times \hat{\mathbf{z}})/l_B^2 \\ \mathbf{b}_2 \equiv 2(\hat{\mathbf{z}} \times \mathbf{a}_1)/l_B^2 \end{cases}. \tag{9}$$

We now introduce magnetic Bloch vectors for quasiparticle eigenstates by[34]

$$\mathbf{k} \equiv \frac{\mu_1}{\mathcal{N}_\mathrm{f}}\mathbf{b}_1 + \frac{\mu_2}{\mathcal{N}_\mathrm{f}}\mathbf{b}_2 \qquad \left(-\frac{\mathcal{N}_\mathrm{f}}{4} < \mu_j \le \frac{\mathcal{N}_\mathrm{f}}{4}\right), \tag{10}$$

and those for the center-of-mass coordinate by

$$\mathbf{q} \equiv \frac{\mu_1}{\mathcal{N}_\mathrm{f}}\mathbf{b}_1 + \frac{\mu_2}{\mathcal{N}_\mathrm{f}}\mathbf{b}_2 \qquad \left(-\frac{\mathcal{N}_\mathrm{f}}{2} < \mu_j \le \frac{\mathcal{N}_\mathrm{f}}{2}\right), \tag{11}$$

where $\mathcal{N}_\mathrm{f}$ is an even integer with $\mathcal{N}_\mathrm{f}^2$ denoting the number of flux quanta in the system. Notice that $\mathbf{q}$ covers an area four times as large as that of $\mathbf{k}$.

C. Landau-level-expansion method (LLX)

It has been shown[34] that the pair potential of the conventional Abrikosov lattice can be expanded in two ways with respect to $(\mathbf{r}_1, \mathbf{r}_2)$ and $(\mathbf{R}, \mathbf{r}) \equiv (\frac{\mathbf{r}_1+\mathbf{r}_2}{2}, \mathbf{r}_1-\mathbf{r}_2)$ as

$$\begin{aligned} &\underline{\Delta}(\mathbf{r}_1, \mathbf{r}_2) \\ &= \sum_{\mathbf{k}\alpha}\sum_{N_1N_2} \underline{\Delta}^{(\mathbf{k}p_z)}_{N_1N_2}\, \psi_{N_1\mathbf{k}\alpha}(\mathbf{r}_1)\, \psi_{N_2\mathbf{q}-\mathbf{k}\alpha}(\mathbf{r}_2)\, \frac{\mathrm{e}^{ip_z(z_1-z_2)}}{L} \\ &= \frac{\mathcal{N}_\mathrm{f}}{\sqrt{2}} \sum_{N_\mathrm{c}} \sum_{N_\mathrm{r} m p_z} (-1)^{N_\mathrm{r}}\, \bar{\underline{\Delta}}^{(N_\mathrm{c}m)}_{N_\mathrm{r}p_z} \psi^{(\mathrm{c})}_{N_\mathrm{c}\mathbf{q}}(\mathbf{R})\, \psi^{(\mathrm{r})}_{N_\mathrm{r}m}(\mathbf{r}) \frac{\mathrm{e}^{ip_z z}}{L}\,. \end{aligned} \tag{12}$$

Here $\psi_{N\mathbf{k}\alpha}$ is a quasiparticle basis function with N denoting the Landau level, $\mathbf{k}$ defined by Eq. (10), and α (=1,2) signifying signifying two-fold degeneracy of every orbital state. On the other hand, $\psi^{(\mathrm{c})}_{N_\mathrm{c}\mathbf{q}}$ and $\psi^{(\mathrm{r})}_{N_\mathrm{r}m}$ are basis functions for the center-of-mass and relative coordinates, respectively, with N_c and N_r denoting the corresponding Landau levels, $\mathbf{q}$ defined by Eq. (11), and m an eigenvalue for the relative orbital angular momentum operator $\hat{l}_z$. The quantities p_z and L are, respectively, the wavenumber and the system length along the z direction parallel to the magnetic field; we adopt a notation of using $\mathbf{p}$ as a *wavevector* in zero field to distinguish it from the two-dimensional magnetic Bloch vector $\mathbf{k}$ perpendicular to the field. As noted in Ref. 39, an arbitrary single $\mathbf{q}$ suffices to describe the conventional Abrikosov lattices due to the broken translational symmetry of the vortex lattice. Then the first expansion of Eq. (12) tells us that, by choosing $\mathbf{q} = \mathbf{0}$, we get an complete analogy with the uniform system in that the pairing occurs between $(\mathbf{k}, p_z)$ and $(-\mathbf{k}, -p_z)$. Finally, the two expansion coefficients $\underline{\Delta}^{(\mathbf{k}p_z)}_{N_1N_2}$ and $\bar{\underline{\Delta}}^{(N_\mathrm{c}m)}_{N_\mathrm{r}p_z}$ are connected by

$$\begin{aligned} \underline{\Delta}^{(\mathbf{k}p_z)}_{N_1N_2} &= \frac{\mathcal{N}_\mathrm{f}}{2} \sum_{N_\mathrm{c}N_\mathrm{r}} \langle N_1N_2|N_\mathrm{c}N_\mathrm{r}\rangle \sum_m \langle 2\mathbf{k}-\mathbf{q}|m+N_\mathrm{r}\rangle \\ &\qquad \times (-1)^{N_\mathrm{r}}\, \bar{\underline{\Delta}}^{(N_\mathrm{c}m)}_{N_\mathrm{r}p_z}\,, \end{aligned} \tag{13a}$$

$$\begin{aligned} \bar{\underline{\Delta}}^{(N_\mathrm{c}m)}_{N_\mathrm{r}p_z} &= \frac{2}{\mathcal{N}_\mathrm{f}} \sum_{N_1N_2} \langle N_\mathrm{c}N_\mathrm{r}|N_1N_2\rangle \sum_{\mathbf{k}} \langle m+N_\mathrm{r}|2\mathbf{k}-\mathbf{q}\rangle \\ &\qquad \times (-1)^{N_\mathrm{r}}\, \underline{\Delta}^{(\mathbf{k}p_z)}_{N_1N_2}\,, \end{aligned} \tag{13b}$$

where $\langle N_1N_2|N_\mathrm{c}N_\mathrm{r}\rangle$ and $\langle 2\mathbf{k}-\mathbf{q}|m+N_\mathrm{r}\rangle$ are elements of unitary matrices for the basis change, i.e. overlap integrals. Their explicit expressions together with those for $\psi_{N\mathbf{k}\alpha}$, $\psi^{(\mathrm{c})}_{N_\mathrm{c}\mathbf{q}}$, and $\psi^{(\mathrm{r})}_{N_\mathrm{r}m}$ are given in Appendix B.

A great advantage of using Eq. (12) is that it enables us to transform Eq. (1) into a numerically tractable problem, as mentioned before. Indeed, expanding the quasiparticle wavefunctions as

$$\mathbf{u}(\mathbf{r}) = \sum_{N\mathbf{k}\alpha p_z} \mathbf{u}_s(N)\, \psi_{N\mathbf{k}\alpha}(\mathbf{r})\, \frac{\mathrm{e}^{ip_z z}}{\sqrt{L}}\,, \tag{14a}$$

$$\mathbf{v}(\mathbf{r}) = \sum_{N\mathbf{k}\alpha p_z} \mathbf{v}_s(N)\, \psi_{N\mathbf{q}-\mathbf{k}\alpha}(\mathbf{r})\, \frac{\mathrm{e}^{-ip_z z}}{\sqrt{L}}\,, \tag{14b}$$

Eq. (1) is reduced to a separate matrix eigenvalue problem for each $\mathbf{k}\alpha p_z$, and the eigenstate is labelled by $s = \nu\mathbf{k}\alpha p_z\sigma$ with ν and σ denoting the quasiparticle band and its spin, respectively. Explicitly, Eq. (1) becomes

$$\sum_{N_2} \begin{bmatrix} \underline{\mathcal{H}}^{(p_z)}_{N_1N_2} & \underline{\Delta}^{(\mathbf{k}p_z)}_{N_1N_2} \\ \underline{\Delta}^{(\mathbf{k}p_z)\dagger}_{N_1N_2} & -\underline{\mathcal{H}}^{(p_z)}_{N_1N_2} \end{bmatrix} \begin{bmatrix} \mathbf{u}_s(N_2) \\ -\mathbf{v}^*_s(N_2) \end{bmatrix} = E_s \begin{bmatrix} \mathbf{u}_s(N_1) \\ -\mathbf{v}^*_s(N_1) \end{bmatrix}, \tag{15}$$

where $\underline{\Delta}^{(\mathbf{k}p_z)}_{N_1N_2}$ is given by Eq. (13a), and $\underline{\mathcal{H}}^{(p_z)}_{N_1N2}$ is diag-

onal as

$$\underline{\mathcal{H}}^{(p_z)}_{N_1N2} = \delta_{N_1N_2}\left[(N_1+\tfrac{1}{2})\hbar\omega_B + \frac{\hbar^2p_z^2}{2m_{\rm e}} - \varepsilon_{\rm F}\right]\underline{1}\,, \quad (16)$$

with $\omega_B \equiv eB/Mc$ the cyclotron frequency.

The self-consistency equation (4) are also simplified greatly. Let us define

$$V_{\mathbf{p}\mathbf{p}'} \equiv \int V(\mathbf{r})\,{\rm e}^{-{\rm i}(\mathbf{p}-\mathbf{p}')\cdot\mathbf{r}}\,{\rm d}^3r$$
$$= 4\pi\sum_{\ell=0}^{\infty}\sum_{m=-\ell}^{\ell}\bar{V}_\ell(p,p')Y_{\ell m}(\hat{\mathbf{p}})Y^*_{\ell m}(\hat{\mathbf{p}}')\,, \quad (17)$$

where $Y_{\ell m}(\hat{\mathbf{p}}) \equiv \Theta_{\ell m}(\theta_{\mathbf{p}})\frac{1}{\sqrt{2\pi}}\exp(im\varphi_{\mathbf{p}})$ is the spherical harmonic.[40] We also expand both $\underline{\Delta}$ and $\underline{\Phi}$ in terms of the center-of-mass and relative coordinates as the last line of Eq. (12). Then Eq. (4) is transformed into an equation for the expansion coefficients of each $(N_{\rm c}, m)$ as

$$\underline{\bar{\Delta}}^{(N_{\rm c}m)}_{N_{\rm r}p_z} = \frac{1}{2\pi l_B^2 L}\sum_{\ell N'_{\rm r}p'_z}\bar{V}_\ell(p,p')\Theta_{\ell m}(\theta_{\mathbf{p}})\Theta_{\ell m}(\theta_{\mathbf{p}'})\underline{\bar{\Phi}}^{(N_{\rm c}m)}_{N'_{\rm r}p'_z} \quad (18)$$

with $p = \sqrt{N_{\rm r}/l_B^2 + p_z^2}$ and $\theta_{\mathbf{p}} = \tan^{-1}\left(\frac{\sqrt{N_{\rm r}}/l_B}{p_z}\right)$.

Let us further assume that a single ℓ is relevant in Eq. (17) and take the corresponding $\bar{V}_\ell(p,p')$ in a separable form as

$$\bar{V}_\ell(p,p') = V_\ell\, W_\ell(\xi)W_\ell(\xi')\,, \quad (19)$$

where $W_\ell(\xi)$ is some cut-off function with respect to $\xi \equiv \hbar^2p^2/2m_{\rm e} - \varepsilon_{\rm F}$ satisfying $W_\ell(0) = 1$. Then can rewrite Eq. (18) as

$$\underline{\bar{\Delta}}^{(N_{\rm c}m)}_{N_{\rm r}p_z} = \underline{\tilde{\Delta}}^{(N_{\rm c}m)}W_\ell(\xi)\Theta_{\ell m}(\theta_{\mathbf{p}})\,, \quad (20a)$$

with $\xi = \hbar^2(N_{\rm r}/l_B^2 + p_z^2)/2m_{\rm e} - \varepsilon_{\rm F}$ and

$$\underline{\tilde{\Delta}}^{(N_{\rm c}m)} = \frac{V_\ell}{2\pi l_B^2 L}\sum_{N'_{\rm r}p'_z}W_\ell(\xi')\Theta_{\ell m}(\theta_{\mathbf{p}'})\,\underline{\bar{\Phi}}^{(N_{\rm c}m)}_{N'_{\rm r}p'_z}\,. \quad (20b)$$

Thus, we only need a self-consistent solution for a set of discrete parameters $\{\underline{\tilde{\Delta}}^{(N_{\rm c}m)}(T,B)\}$ through Eqs. (15) and (20) using Eq. (13).

It has been shown[39,41] that retaining a few $N_{\rm c}$'s, e.g., $N_{\rm c} = 0, 6, 12$ for the hexagonal lattice, is sufficient to describe the vortex lattices of $H \gtrsim 0.05H_{c2}$. Thus, the original problem of obtaining self-consistency for $\underline{\Delta}(\mathbf{r}_1, \mathbf{r}_2)$ at all space points is now reduced to the one for a few expansion coefficients $\{\underline{\tilde{\Delta}}^{(N_{\rm c}m)}(T,B)\}$. This situation is analogous to the zero-field case where a single parameter $\Delta_0(T)$ specifies the pair potential.

The linearized self-consistency equation is obtained by substituting into Eq. (20b) the expression of $\underline{\bar{\Phi}}^{(N_{\rm c}m)}_{N_{\rm r}p_z}$ linear in the pair potential:[34]

$$\underline{\bar{\Phi}}^{(N_{\rm c}m)}_{N_{\rm r}p_z} = -\frac{1}{2}\sum_{N_1N_2}\langle N_{\rm c}N_{\rm r}|N_1N_2\rangle\,\frac{\tanh\frac{\xi_1}{2T}+\tanh\frac{\xi_2}{2T}}{\xi_1+\xi_2}$$
$$\times\sum_n(-1)^n\langle N_1N_2|N_{\rm c}+n\,N_{\rm r}-n\rangle\,\underline{\bar{\Delta}}^{(N_{\rm c}+n\,m+n)}_{N_{\rm r}-n\,p_z}\,. \quad (21)$$

Equation (20) with Eq. (21) determines the mean-field $H_{c2}(T)$, i.e. $T_c(H)$. If we use the asymptotic expression (B6) for the overlap integral $\langle N_{\rm c}N_{\rm r}|N_1N_2\rangle$ and replace the sum over N_1 by the integral over $x \equiv (N_1 - N_2)/\sqrt{2(N_{\rm c}+N_{\rm r})}$, we reproduce the smooth quasiclassical $H_{c2}^{\rm quasi}(T)$ obtained, for example, for the s-wave pairing by Helfand and Werthamer.[42]

Finally, Eq. (4) for two-dimensional systems can be transformed similarly. It is also obtained from Eqs. (17)-(20) by replacing $V_\ell(p,p') \to V^{(m)}(p,p')$, extending the summation over m in Eq. (17) from $-\infty$ to ∞, and finally restricting the summation over ℓ and p_z only to $\ell = 0$ and $p_z = 0$, respectively.

III. TWO-DIMENSIONAL CALCULATIONS

We first consider a couple of two-dimensional models and perform fully self-consistent calculations. Our purposes in this section are summarized as follows: (i) to clarify the essential features of the results by self-consistent calculations; (ii) to see whether point nodes in the gap really enhances the dHvA signals as Miyake claims.[19]

A. Models

The one-particle Hamiltonian (2) yields an isotropic Fermi surface specified by a unit vector $\hat{\mathbf{p}} = (\cos\varphi_{\mathbf{p}}, \sin\varphi_{\mathbf{p}})$. As for the pairing interaction (17), we adopt the following models:

$$V_{\mathbf{p}\mathbf{p}'} = \begin{cases} V_0\, W(\xi)W(\xi') \\ V_2\, W(\xi)(\hat{\mathbf{p}}_x^2 - \hat{\mathbf{p}}_y^2)\, W(\xi')(\hat{\mathbf{p}}_x'^2 - \hat{\mathbf{p}}_y'^2) \end{cases}, \quad (22)$$

where

$$W(\xi) = \exp\left[-\frac{1}{2}\left(\frac{\xi}{\hbar\omega_{\rm D}}\right)^4\right] \quad (23)$$

is a smooth cut-off function with $\omega_{\rm D}$ a cut-off frequency. The second model of Eq. (22) is beyond the original isotropic interaction (17), but it is convenient for the above-mentioned purposes. In zero field, the two interactions yield the s- and $d_{x^2-y^2}$-wave gaps as

$$\underline{\Delta}_{\mathbf{p}} = \begin{cases} \Delta_0 W(\xi)\, i\underline{\sigma}_2 & : s\text{-wave} \\ \Delta_0 W(\xi)(\hat{\mathbf{p}}_x^2 - \hat{\mathbf{p}}_y^2)\, i\underline{\sigma}_2 & : d_{x^2-y^2}\text{-wave} \end{cases}, \quad (24)$$

respectively. The corresponding $\underline{\bar{\Delta}}^{(N_c m)}_{N_r}$ of Eq. (20) for $\mathbf{B}\,\|\,\hat{\mathbf{z}}$ is given by

$$\underline{\bar{\Delta}}^{(N_c m)}_{N_r} = \begin{cases} \tilde{\Delta}^{(N_c)} W(\xi)\, \delta_{m0}\, i\underline{\sigma}_2 \\ \tilde{\Delta}^{(N_c)} W(\xi) \dfrac{\delta_{m2}+\delta_{m-2}}{2}\, i\underline{\sigma}_2 \end{cases}, \tag{25a}$$

with $\xi \equiv \hbar^2 N_r/2m_e l_B^2 - \varepsilon_F$ and

$$\tilde{\Delta}^{(N_c)} = \begin{cases} \dfrac{V_0}{4\pi l_B^2} \displaystyle\sum_{N_r'} W_\ell(\xi')\, \bar{\Phi}^{(N_c,0)}_{N_r'} \\ \dfrac{V_2}{4\pi l_B^2} \displaystyle\sum_{N_r'} W_\ell(\xi')\, \dfrac{\bar{\Phi}^{(N_c,2)}_{N_r'} + \bar{\Phi}^{(N_c,-2)}_{N_r'}}{2} \end{cases}. \tag{25b}$$

Here we have adopted a normalization for $\tilde{\Delta}^{(N_c)}$ different from Eq. (20) so that $\tilde{\Delta}^{(N_c)}$ acquires a direct correspondence to the maximum gap Δ_0 in Eq. (24); the factor $\frac{1}{2}$ in the second case stems from $\cos 2\varphi_{\mathbf{p}}$ in Eq. (24).

We have chosen V_ℓ in Eq. (22) as

$$g_\ell \equiv -N(0)V_\ell = 0.5\,, \tag{26}$$

where $N(0) = m_e/2\pi\hbar^2$ is the density of states per spin at the Fermi level. Another important parameter is the zero-temperature coherence length defined by

$$\xi_0 \equiv \hbar v_F/\Delta_0\,, \tag{27}$$

with v_F the Fermi velocity. We have adopted $p_F\xi_0 = 5$ for our calculations. The above two quantities fix our models completely; the cut-off $\hbar\omega_D$ in Eq. (23) and $T_c(B=0)$ are calculated using the gap equation.

It should be noted that choosing $p_F\xi_0$ also determines the following quantities: (i) the ratio $\hbar\omega_{H_{c2}^{\rm quasi}}/k_B T_c$, where $\hbar\omega_{H_{c2}^{\rm quasi}}$ is the zero-temperature cyclotron energy at the quasiclassical upper critical field $H_{c2}^{\rm quasi}$; (ii) the number N_F of the Landau levels below the Fermi level at $H_{c2}^{\rm quasi}$. Indeed, using the usual cut-off model $W(\xi) = \theta(\hbar\omega_D - |\xi_{\mathbf{p}}|)$ with θ the step function, we obtain the following results for the s-wave pairing:

$$\begin{cases} \hbar\omega_{H_{c2}^{\rm quasi}}/k_B T_c = 6.28/p_F\xi_0\,, \\ N_F \equiv \varepsilon_F/\hbar\omega_{H_{c2}^{\rm quasi}} = 0.140(p_F\xi_0)^2\,. \end{cases} \tag{28}$$

To reproduce the experimental situation $\hbar\omega_{H_{c2}^{\rm quasi}}/k_B T_c = 1 \sim 3$ within the present model, we should go into the quantum limit $p_F\xi_0 = 6 \sim 2$, but we then have $N_F = 5 \sim 1$. In real materials, however, $\hbar\omega_{H_{c2}^{\rm quasi}}/k_B T_c$ and $p_F\xi_0$ are apparently independent parameters due to effects not covered by the free-particle model such as the energy band structure. Indeed, $p_F\xi_0$ is of the order of 30 ($NbSe_2$) or even larger, whereas $\hbar\omega_{H_{c2}^{\rm quasi}}/k_B T_c = 1 \sim 3$; see Table I below. Also, $N_F \gg 1$ for those materials. The failures to describe these situations are among the main difficulties of the free-particle model of Eq. (2).

Motivated by these observations, we also perform another calculations with much more Landau levels below the Fermi level. This is achieved by including the effect of the band dispersion. Specifically, we apply the Onsager-Lifshiz (OL) quantization scheme to $\underline{\mathcal{H}}$ of Eq. (1), i.e. the procedure which has been very successful for describing the dHvA oscillations in the normal state.[1,2] Given the density of states per spin $N(\varepsilon)$ and the average flux density B, the Nth Landau level ε_N ($N = 0, 1, 2, \cdots$) is determined by

$$2\left(N + \frac{1}{2}\right)\frac{\hbar^2}{l_B^2} = 4\pi\hbar^2 \int_0^{\varepsilon_N} N(\varepsilon')\, d\varepsilon'\,. \tag{29}$$

We fix $\underline{\mathcal{H}}^{(p_z)}_{N_1 N_2}$ of Eq. (15) in this way assuming it is diagonal. In contrast, we use the same expression for $\underline{\Delta}^{(\mathbf{k}p_z)}_{N_1 N_2}$ of Eq. (15) as the free-particle case. Finally, we choose $\xi = \varepsilon_{N_r/2} - \varepsilon_F$ in Eq. (25) based on the consideration of the free-particle model.[34] With these prescriptions together with the transformation (13), the coupled equations (15) and (25) are defined unambiguously. We adopt the model density of states:

$$N(\varepsilon) = \frac{m_e}{2\pi\hbar^2}\left(1 + \frac{\alpha\Gamma}{\varepsilon^2 + \Gamma^2}\right), \tag{30}$$

and choose the numerical constants $(\alpha, \Gamma) = (2.1, 2.7)$ and $(5.0, 1.0)$ for the s- and d-wave models of Eq. (24), respectively. We also use Eq. (26) for the pairing interaction and fix $\hbar\omega_D = 0.5\varepsilon_F$ in Eq. (23). We thereby obtain $\hbar\omega_{H_{c2}^{\rm quasi}} \approx k_B T_c$ at $T = 0$ and $N_F \sim 30$ at $H = H_{c2}^{\rm quasi}$, which describe the experimental situation much better than the free-particle model.

B. Numerical procedures

Coupled equations (15) and (25) are solved iteratively with the help of the transformation (13) to obtain self-consistent $\{\tilde{\Delta}^{(N_c)}\}$'s and the corresponding quasiparticle eigenstates. The hexagonal (square) vortex lattice is assumed for the s-wave ($d_{x^2-y^2}$-wave) model, as expected theoretically in high magnetic fields[43,44] and observed recently in $La_{1.83}Sr_{0.17}CuO_{4+\delta}$.[45] It should be noted, however, that the precise lattice structure is not important for the theory of the dHvA oscillation in superconductors. We set $\mathbf{q} = \frac{1}{2}(\mathbf{b}_1 + \mathbf{b}_2)$ in the relevant equations so that a core of the pair potential is located at the origin $\mathbf{R} = \mathbf{0}$.[39] An advantage of this choice is that the corresponding quasiparticle energies have the rotational symmetry of the hexagonal (square) lattice around $\mathbf{k} = \mathbf{0}$; other choices would shift the rotation axis from the origin. We then perform calculations of Eqs. (15) and (25) for a set of discrete $\mathbf{k}$'s defined by Eq. (10), where $\mathcal{N}_f$ is chosen as a multiple of 12 to include all the high-symmetry points Γ, M, and K (Γ, X, and M) of the hexagonal (square) lattice. Three different values $\mathcal{N}_f = 12, 24, 36$ are used to see the size dependence, and it has been checked that the results do not differ for the three cases. The hexagonal (square) symmetry enables us to restrict the summation

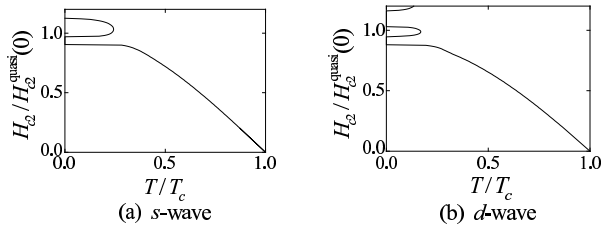

FIG. 1: The upper critical field H_{c2} as a function of T for (a) s-wave and (b) d-wave of Eq. (24). Here $p_{\rm F}\xi_0 = 5$, and H_{c2} is normalized by the quasiclassical upper critical field $H_{c2}^{\rm quasi}(T=0)$.

over $\mathbf{k}$ into approximately 1/12 (1/8) area of the Brillouin zone. Thus, the calculations can be reduced greatly with due care on the degeneracy of high-symmetry points. Finally, the obtained eigenvalues and eigenstates are substituted into Eq. (6) to calculate the magnetization by Eq. (7). All the calculations are performed at $T=0.1T_c$.

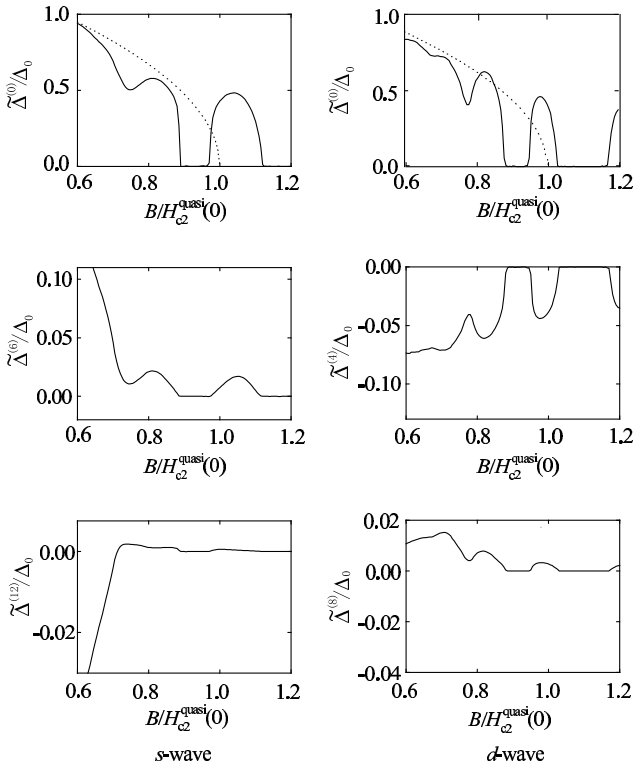

FIG. 2: The expansion coefficients $\tilde{\Delta}^{(N_{\rm c})}$ in Eq. (25) as a function of B for the s-wave (first column) and the d-wave (second column) with $T = 0.1T_c$ and $p_{\rm F}\xi_0 = 5$. The dotted lines in the first row signify the square-root behavior expected from the quasiclassical theory.

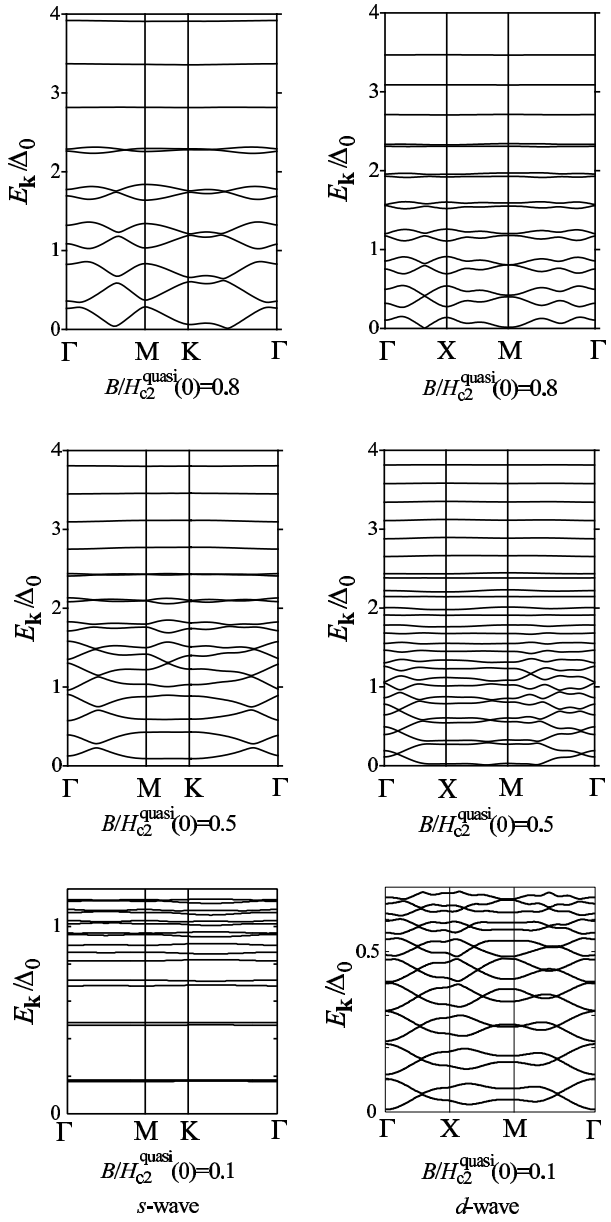

FIG. 3: Quasiparticle dispersion in the magnetic Brillouin zone for the s-wave hexagonal lattice (first column) and the d-wave square lattice (second column). Here $p_{\rm F}\xi_0 = 5$, $T = 0.1T_c$, and $B/H_{c2}^{\rm quasi}(0)$ is equal to 0.8, 0.5, and 0.1 from top to bottom, respectively

C. Results

The above self-consistent procedure is known to give rise to oscillatory singular behaviors in both H_{c2} and $\tilde{\Delta}^{(N_{\rm c})}$ in the field range where the dHvA oscillation persists.[46,47,48] Figure 1 displays $H_{c2}(T)$ calculated self-consistently for the s- and d-wave models; it is normalized by the quasiclassical upper critical field $H_{c2}^{\rm quasi}(T=0)$. An oscillatory behavior sets in around $T \lesssim 0.2T_c$, and H_{c2} deviates substantially from the smooth Helfand-

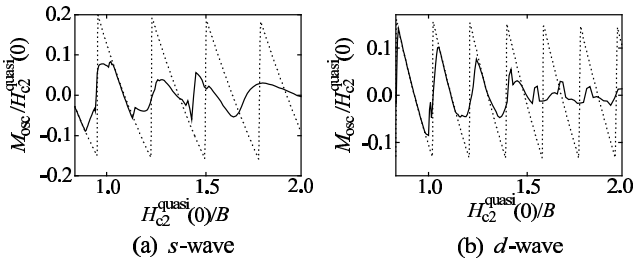

FIG. 4: Oscillatory part of magnetization $M_{\rm osc}$ for (a) the s-wave and (b) the d-wave, over $0.8 \le H_{c2}^{\rm quasi}(0)/B \le 2.0$ ($1.2 \ge B/H_{c2}^{\rm quasi}(0) \ge 0.5$) with $T = 0.1T_c$ and $p_{\rm F}\xi_0 = 5$. The dotted lines are the curves of the corresponding normal state.

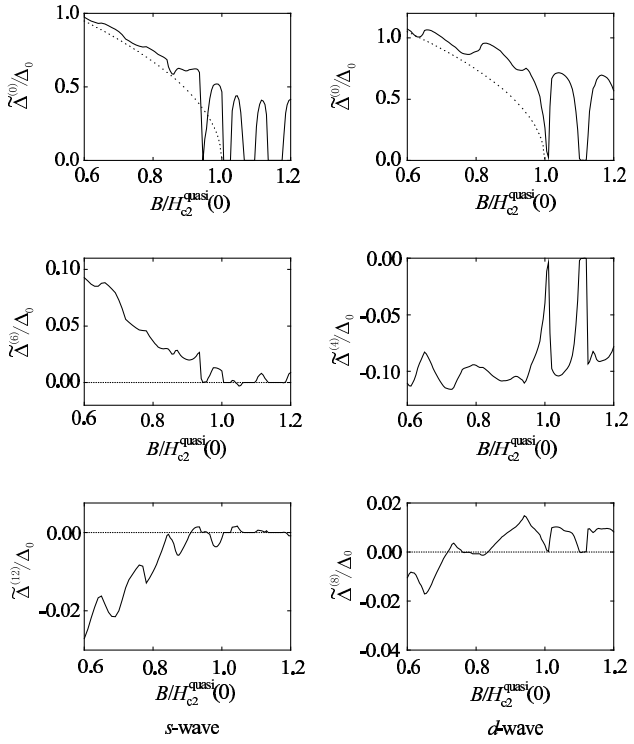

FIG. 5: The expansion coefficients $\tilde{\Delta}^{(N_{\rm c})}$ in Eq. (25) as a function of B for the s-wave (first column) and the d-wave (second column). Here $T = 0.1T_c$, and the non-quadratic dispersion given by Eq. (30) is used. The dotted lines in the first row signify the square-root behavior expected from the quasiclassical theory.

Werthamer behavior[42] predicted by the quasiclassical theory. The number of the Landau levels below the Fermi level is $N_{\rm F} \sim 10$ around $H_{c2}^{\rm quasi}(0)$, which is considerably smaller than those for the real materials. Figure 2 shows $\tilde{\Delta}^{(N_{\rm c})}$ as a function of B at $T = 0.1T_c$ for the s-wave hexagonal lattice (first column) and the d-wave square lattice (second column); they are real and finite only for $N_{\rm c} = 0, 6, 12, \cdots$ $(0, 4, 8, \cdots)$ for the hexagonal (square) lattice,[39,41] as already mentioned. We observe that $\tilde{\Delta}^{(N_{\rm c})}$'s are also singular, and the dominant $\tilde{\Delta}^{(0)}$ component cannot be described by the square-root behavior near $H_{c2}^{\rm quasi}(0)$ expected from the quasiclassical theory. However, those singular behaviors disappear gradually as B decreases.

Figure 3 displays the quasiparticle energies in the magnetic Brillouin zone for the s-wave hexagonal lattice (first column) and the d-wave square lattice (second column) at $B/H_{c2}^{\rm quasi}(0) = 0.8$, 0.5, and 0.1. At $B/H_{c2}^{\rm quasi}(0) = 0.8$, we already observe large dispersion for $E \lesssim 2\Delta_0$ where the pair potential is effective. In contrast, the flat Landau-level structure remains for $E \gtrsim 2\Delta_0$ where the pair potential vanishes in the present cut-off model of Eq. (23). Thus, the dispersion is caused clearly by the scattering from the growing pair potential, and as will be discussed below, it is the origin of the extra dHvA oscillation damping in the vortex state. We also notice that, for $B/H_{c2}^{\rm quasi}(0) \gtrsim 0.5$, almost no qualitative difference can be seen between the s- and d-wave cases. At a lower field of $B/H_{c2}^{\rm quasi}(0) = 0.1$, however, a marked difference grows around $E \lesssim \Delta_0$. The s-wave energy bands of $E \lesssim 0.7\Delta_0$ are flat and occur in pairs with the level spacing of the order of $\Delta_0^2/\varepsilon_{\rm F}$. As already pointed out by Norman *et al.*,[29] these corresponds to the bound core states of an isolated vortex with little tunneling probability between adjacent cores. In contrast, the d-wave bands in the same region are densely packed with large dispersion, indicating the extended nature of the corresponding quasiparticle wavefunctions. From this comparison, we conclude that no bound states exist for the d-wave model even in the zero-field limit of an isolated vortex, in agreement with the result of Franz and Tešanović.[49] This difference in the low-energy dispersion at low fields was already reported in Ref. 35.

Figure 4 shows oscillatory part of the magnetization $M_{\rm osc}$ calculated numerically by Eq. (7), where curves of the corresponding normal state are also plotted for comparison. The damping starts from above $H_{c2}^{\rm quasi}(0)$ where $\tilde{\Delta}^{(0)}$ is already finite as in Fig. 2, and develops rapidly as $\tilde{\Delta}^{(0)}$ grows in decreasing B. Thus, the mean-field theory predicts that the dHvA oscillation comes together with the oscillatory singular behaviors in H_{c2} and $\tilde{\Delta}^{(N_{\rm c})}$. Combined with the energy dispersion given in Fig. 3, we are now able to attribute the origin of the extra damping unambiguously to the Landau-level broadening due to the pair potential. The oscillations are rather irregular in both the s-wave and d-wave cases, in accordance with the singular behaviors of $\Delta^{(N_{\rm c})}$ in Fig. 2. We also see no qualitative difference between the two cases.

However, the free-particle model has several inappropriate points as discussed already around Eq. (28). For example, the number of Landau levels below the Fermi level $N_{\rm F}$ is necessarily $N_{\rm F} \sim 10$ at $H_{c2}^{\rm quasi}$ for $p_{\rm F}\xi_0 = 5$, which is much smaller than the values of the materials displaying the dHvA oscillation. Hence the above numerical results may not be sufficient to say anything quantitative about the dHvA attenuation or the differences between the s- and d-wave cases. We have thus

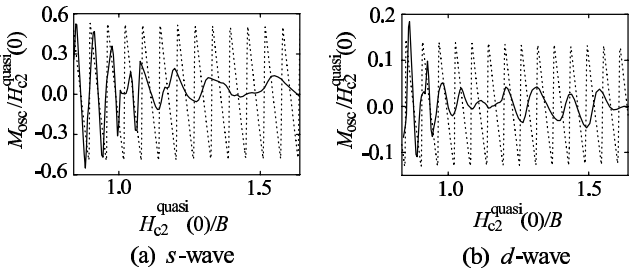

FIG. 6: Oscillatory part of magnetization $M_{\rm osc}$ for (a) the s-wave and (b) the d-wave, over $0.8 \lesssim H_{c2}^{\rm quasi}(0)/B \leq 1.7$, i.e. $1.25 \gtrsim B/H_{c2}^{\rm quasi}(0) \geq 0.59$. Here $T = 0.1T_c$, and a non-quadratic dispersion given by Eq. (30) is used. The dotted lines are the curves of the corresponding normal state.

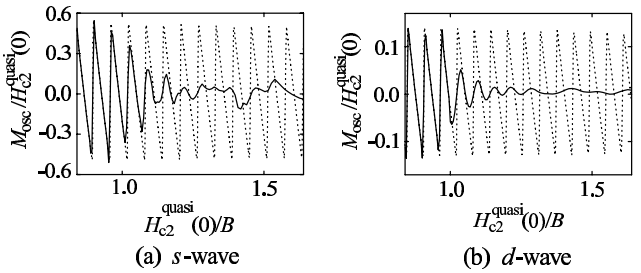

FIG. 7: Oscillatory part of magnetization $M_{\rm osc}$ for (a) the s-wave and (b) the d-wave. The difference from Fig. 7 lies in the use of quasiclassical $\Delta^{(0)}$'s given by the dotted lines in Fig. 5.

performed another calculations for the model described around Eqs. (29) and (30) where $\hbar\omega_{H_{c2}^{\rm quasi}}/k_{\rm B}T_c \sim 1$ and $N_{\rm F} \sim 30$ at $B = H_{c2}^{\rm quasi}(0)$.

Figure 5 shows the field-dependence of the expansion coefficients $\tilde{\Delta}^{(N_{\rm c})}$ calculated self-consistently for the s-wave hexagonal lattice (first column) and the d-wave square lattice (second column). Singular oscillatory behaviors are manifest in both cases as in the case of the quadratic dispersion, which originate from the singular density of states of Landau levels.[48] For example, the dominant $\tilde{\Delta}^{(0)}$ component have a nonzero value from above $H_{c2}^{\rm quasi}$ and deviates substantially from the quasiclassical square-root behavior (dotted lines).

Figure 6 displays the corresponding oscillatory part of the magnetization $M_{\rm osc}$ calculated numerically by Eq. (7), where normal-state results (dotted lines) are also plotted for comparison. The main features are summarized as follows: (i) The oscillations are seen to decrease from above the quasiclassical $H_{c2}^{\rm quasi}$, due to the reentrant behavior of $\tilde{\Delta}^{(N_{\rm c})}$, to be reduced considerably around $B \sim 0.8H_{c2}^{\rm quasi}$, i.e. $H_{c2}^{\rm quasi}/B \sim 1.25$. However, they do not disappear completely in lower fields. (ii) This extra attenuation is due to the broadening of the Landau levels caused by the pair potential, as in the case of the quadratic dispersion. Indeed, we have obtained quasiparticle spectra similar to those of Fig. 3. (iii) The period of the oscillation remains unchanged above $\sim 0.8H_{c2}^{\rm quasi}$, but some irregularity appears in lower fields. These features are in agreement with the results by Norman *et al.*[29] (iv) Little difference can be seen between the s- and d-wave attenuations.

D. Summary of Two-Dimensional Calculations

Let us summarize results and conclusions from our two-dimensional calculations. (i) Combining Figs. 3 and 4, we are now able to attribute the origin of the extra dHvA oscillation damping unambiguously to the Landau-level broadening due to the scattering by the pair potential. (ii) As may be realized from Fig. 6, presence of point nodes along the extremal orbit does not weaken the attenuation, contrary to the statement by Miyake.[19] This fact suggests that the attenuation is determined by the average gap along the extremal orbit. (iii) The mean-field theory predicts that the dHvA oscillation comes together with the oscillatory behaviors in H_{c2} and $\tilde{\Delta}^{(N_{\rm c})}$. This will be so in three dimensional models where $H_{c2}(T)$ also shows an oscillatory behavior.[48] However, such singular behaviors of H_{c2} have never been identified definitely in any materials displaying the dHvA oscillation, and reported H_{c2} curves show more or less the smooth quasiclassical behavior. This discrepancy between the mean-field theory and the dHvA experiments remains a puzzle to be resolved in the future. (iv) The oscillation attenuates considerably around $B \sim 0.8H_{c2}^{\rm quasi}$, i.e. $H_{c2}^{\rm quasi}/B \sim 1.25$, although we have set $\hbar\omega_{H_{c2}^{\rm quasi}}/k_{\rm B}T_c \sim 1$ and $N_{\rm F} \gg 1$ at $H_{c2}^{\rm quasi}$. Thus, the two dimensional models fail to explain the experiment by Terashima *et al.*[9] which shows a persistent oscillation down to $0.2H_{c2}$. In addition, the models cannot say anything about whether presence of a line node along the extremal orbit weakens the attenuation. (v) The approximation of retaining only $\tilde{\Delta}^{(0)}$ works excellently for calculating $M_{\rm osc}$. Indeed, we have checked that the curves of $M_{\rm osc}$ thereby obtained are almost indistinguishable from those of Fig. 6. (vi) The discrepancy mentioned in (iii) above suggests that we should rather use $\tilde{\Delta}^{(0)}$ obtained quasiclassically to reproduce the smooth behaviors of H_{c2} in real materials. Figure 7 plots curves of $M_{\rm osc}$ calculated using quasiclassical $\tilde{\Delta}^{(0)}$, i.e. the dotted lines of Fig. 5. The oscillations are seen more regular than those of Fig. 6, but the amplitudes attenuate almost similarly and are reduced considerably around $H_{c2}^{\rm quasi}/B \sim 1.25$. We hence realize that using the quasiclassical $\tilde{\Delta}^{(0)}$ suffices for the theory of the oscillation damping. This statement is especially true in the low-field region $\sim 0.2H_{c2}^{\rm quasi}$ where $\tilde{\Delta}^{(0)}$ approaches to the quasiclassical behavior, as may be realized from Fig. 5.

IV. THREE-DIMENSIONAL CALCULATIONS

Having clarified basic features of the dHvA oscillation for two-dimensional models as well as the mechanism of the extra oscillation damping, we proceed to consider three-dimensional models with various gap structures which are more relevant to real materials. Our purposes in this section are summarized as follows: (i) to clarify the connection between the extra dHvA oscillation damping and the gap anisotropy by numerical calculations; (ii) to obtain an analytic formula for the extra oscillation damping; (iii) to estimate the gap magnitudes of various materials using the obtained analytic formula.

A. Model

The one-particle Hamiltonian (2) yields a spherical Fermi surface in the normal state. As for the pairing interaction, we consider three different models:

$$V_{\mathbf{p}\mathbf{p}'} = \begin{cases} V_0\, W(\xi)W(\xi') \\ V_2\, W(\xi)(\hat{\mathbf{p}}_x^2-\hat{\mathbf{p}}_y^2)\, W(\xi')(\hat{\mathbf{p}}_x'^2-\hat{\mathbf{p}}_y'^2) \\ V_1\, W(\xi)\, \hat{\mathbf{p}}\cdot\hat{\mathbf{c}}\, W(\xi')\, \hat{\mathbf{p}}'\cdot\hat{\mathbf{c}} \end{cases} . \quad (31)$$

Here $W(\xi)$ is a cut-off function given by Eq. (23), $\hat{\mathbf{p}} \equiv (\sin\theta_{\mathbf{p}}\cos\varphi_{\mathbf{p}}, \sin\theta_{\mathbf{p}}\sin\varphi_{\mathbf{p}}, \cos\theta_{\mathbf{p}})$ specifies a point on the Fermi surface, and $\hat{\mathbf{c}} \equiv (\sin\theta_{\mathbf{c}}, 0, \cos\theta_{\mathbf{c}})$ denotes the direction of the crystal c-axis, in the coordinate frame where $\mathbf{B} \parallel \hat{\mathbf{z}}$. Again the latter two models of Eq. (31) are beyond the original spherical interaction (17), but they are convenient for the above-mentioned purposes. In zero field, Eq. (31) yield

$$\underline{\Delta}_{\mathbf{p}} = \begin{cases} \Delta_0 W(\xi)\, i\underline{\sigma}_2 & : s\text{-wave} \\ \Delta_0 W(\xi)(\hat{\mathbf{p}}_x^2-\hat{\mathbf{p}}_y^2)\, i\underline{\sigma}_2 & : d_{x^2-y^2}\text{-wave} \\ \Delta_0 W(\xi)\, \hat{\mathbf{p}}\cdot\hat{\mathbf{c}}\; i\underline{\sigma}_3\underline{\sigma}_2 & : p_z\text{-wave} \end{cases} , \quad (32)$$

which denote the isotropic s-wave state, a three-dimensional $d_{x^2-y^2}$-wave state with four point nodes in the extremal orbit perpendicular to $\mathbf{B}$, and the p-wave polar state with a line node perpendicular to $\hat{\mathbf{c}}$, respectively. The corresponding $\bar{\underline{\Delta}}^{(N_{\rm c}m)}_{N_{\rm r}p_z}$ in Eq. (18) can be written as

$$\bar{\underline{\Delta}}^{(N_{\rm c}m)}_{N_{\rm r}p_z} = \begin{cases} \tilde{\Delta}^{(N_{\rm c})} W(\xi)\, \delta_{m0}\, i\underline{\sigma}_2 \\ \tilde{\Delta}^{(N_{\rm c})} W(\xi) \sin^2\theta_{\mathbf{p}}\, \dfrac{\delta_{m2}+\delta_{m-2}}{2}\, i\underline{\sigma}_2 \\ \tilde{\Delta}^{(N_{\rm c})} W(\xi) \Big[\cos\theta_{\mathbf{p}}\cos\theta_{\mathbf{c}}\, \delta_{m0} \\ \quad + \sin\theta_{\mathbf{p}}\sin\theta_{\mathbf{c}}\, \dfrac{\delta_{m1}+\delta_{m-1}}{2} \Big] i\underline{\sigma}_3\underline{\sigma}_2 \end{cases} , \quad (33a)$$

where $\xi \equiv \hbar^2(N_{\rm r}/l_B^2 + p_z^2)/2m_{\rm e} - \varepsilon_{\rm F}$, $\theta_{\mathbf{p}} \equiv \tan^{-1}\!\big(\frac{\sqrt{N_{\rm r}}/l_B}{p_z}\big)$, and $\tilde{\Delta}^{(N_{\rm c})}$ is defined by

$$\tilde{\Delta}^{(N_{\rm c})} = \begin{cases} \dfrac{V_0}{4\pi l_B^2} \displaystyle\sum_{N_{\rm r}'p_z'} W_\ell(\xi')\, \bar{\Phi}^{(N_{\rm c},0)}_{N_{\rm r}'p_z'} \\ \dfrac{V_2}{4\pi l_B^2} \displaystyle\sum_{N_{\rm r}'p_z'} W_\ell(\xi') \sin^2\theta_{\mathbf{p}'}\, \dfrac{\bar{\Phi}^{(N_{\rm c},2)}_{N_{\rm r}'p_z'} + \bar{\Phi}^{(N_{\rm c},-2)}_{N_{\rm r}'p_z'}}{2} \\ \dfrac{V_1}{4\pi l_B^2} \displaystyle\sum_{N_{\rm r}'p_z'} W_\ell(\xi') \Big[\cos\theta_{\mathbf{p}'}\cos\theta_{\mathbf{c}}\, \bar{\Phi}^{(N_{\rm c},0)}_{N_{\rm r}'p_z'} \\ \quad + \sin\theta_{\mathbf{p}'}\sin\theta_{\mathbf{c}}\, \dfrac{\bar{\Phi}^{(N_{\rm c},1)}_{N_{\rm r}'p_z'} + \bar{\Phi}^{(N_{\rm c},-1)}_{N_{\rm r}'p_z'}}{2} \Big] \end{cases} . \quad (33b)$$

Here we have adopted a normalization for $\tilde{\Delta}^{(N_{\rm c})}$ different from Eq. (20) so that this quantity acquires a direct correspondence to the maximum gap Δ_0 in Eq. (32). The factors $\frac{1}{2}$ in the second and third cases stem from $\cos 2\varphi_{\mathbf{p}}$ and $\cos\varphi_{\mathbf{p}}$ in Eq. (32), respectively.

The coefficients $\Delta^{(N_{\rm c})} = \Delta^{(N_{\rm c})}(B,T)$ in Eq. (33) completely specify the pair potential, as already mentioned. Based on the reasoning given in Sec. III D(vi), we here adopt a quasiclassical $\tilde{\Delta}^{(N_{\rm c})}$ rather than the fully self-consistent one. Then the dominant $\tilde{\Delta}^{(0)}$ near H_{c2} follows the mean-field square-root behavior to an excellent approximation:

$$\tilde{\Delta}^{(0)} = a(1 - B/H_{c2})^{1/2} . \quad (34)$$

See the dotted lines in Figs. 2 and 5, for example. In addition, other components $\tilde{\Delta}^{(N_{\rm c}>0)}$ can be neglected for the relevant region $B \gtrsim 0.1H_{c2}$, as pointed out in Sec. III D(v). We hence use the lowest-Landau-level approximation of retaining only $\tilde{\Delta}^{(0)}$. The coefficient $a = a(T)$ in Eq. (34) is determined by requiring that the maximum of

$$\frac{1}{\mathcal{V}} \int d\mathbf{R} \left| \int d\mathbf{r}\, \Delta(\mathbf{r}_1,\mathbf{r}_2)\, {\rm e}^{-i\mathbf{p}\cdot\mathbf{r}/\hbar} \right|^2 \quad (35)$$

be equal to $\Delta_0^2(1 - B/H_{c2})$, where $\Delta_0(T)$ denotes the maximum gap obtained from the weak-coupling theory. This procedure yields

$$a \approx \sqrt{0.5} , \quad (36)$$

for all the three cases of Eq. (33). Substituting Eq. (34) into Eq. (13a) with the choice $\hbar\omega_{\rm D} \sim 10\Delta_0(T=0)$, the off-diagonal elements of Eq. (15) are fixed completely.

The above non-self-consistent procedure has another advantage that we can choose $\hbar\omega_{B=H_{c2}}$ and $\varepsilon_{\rm F}$ in Eq. (16) independently. We have set

$$\hbar\omega_{H_{c2}} = k_{\rm B}T_c \quad \text{at } T = 0 , \quad (37)$$

in accordance with $\hbar\omega_{H_{c2}}/k_{\rm B}T_c = 1 \sim 3$ and $N_{\rm F} \gg 1$ for relevant materials (see Table I below). Also, we have

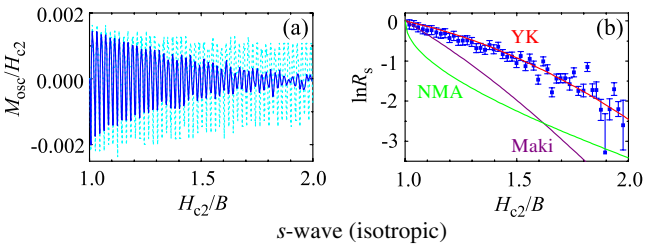

FIG. 8: (a) The oscillatory part of the magnetization $M_{\rm osc}$ in the vortex state (blue line) as compared with the normal-state one (sky-blue line) for the s-wave model of Eq. (32) at $T=0$. (b) The corresponding Dingle plot (points with error bars) as compared with various theoretical predictions; see text for details.

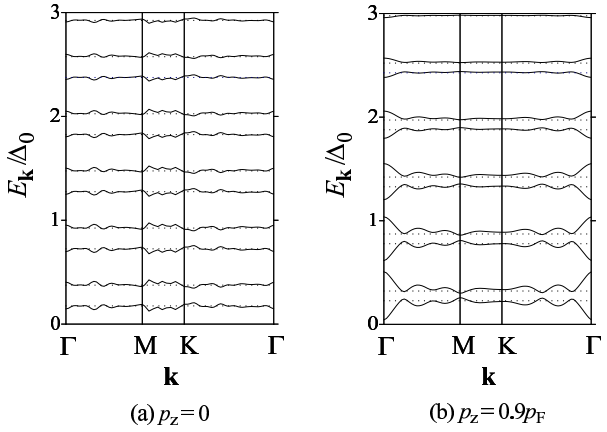

FIG. 9: Quasiparticle dispersion in the magnetic Brillouin zone for the s-wave model at $B=0.968H_{c2}$. (a) p_z=0; (b) p_z=0.9$p_{\rm F}$.

chosen $\varepsilon_{\rm F}$ in such a way that there are about 50 Landau levels below $\varepsilon_{\rm F}$ for the extremal orbit at H_{c2}. Now, the matrix elements of Eq. (15) are specified completely. Hexagonal, square, and hexagonal lattices are assumed for the three cases of Eq. (33), respectively.

B. Numerical Procedures

The wavevector p_z of $0\le p_z\le 1.2p_{\rm F}$ is discretized into $\sim$1000 points with an equal interval. For each of them, we have diagonalized Eq. (15) with the same procedure as described in Sec. III B. The obtained results are substituted into Eq. (6) to calculate the magnetization by Eq. (7). All the calculations are performed at $T=0$.

C. Numerical Results

We first focus on the dHvA oscillation of the s-wave model in Eq. (32) to clarify its basic features. Using our numerical data, we also test the applicability of various theoretical formulas presented so far.

Figure 8(a) presents oscillation of the s-wave magnetization (blue line) as compared with the normal-state one (sky-blue line). With $\hbar\omega_{H_{c2}}=k_{\rm B}T_c$, the oscillation is observed to persist down to a fairly low field of $H_{c2}/B\lesssim 1.8$, i.e., $B\gtrsim 0.55H_{c2}$, which is smaller than $0.8H_{c2}$ around which $\hbar\omega_B$ becomes equal to the spatial average of the energy gap, Eq. (35). This is partly because the gap is smaller within the extremal orbit, as shown quasiclassically by Brandt *et al.*[31] Indeed, Fig. 9 calculated at $B=0.968H_{c2}$ demonstrates that the dispersion for $p_z=0$ is smaller than that for $p_z=0.9p_{\rm F}$. This tendency remains in the high-field region of $B\gtrsim 0.5H_{c2}$.

It has become conventional to express this extra attenuation in the vortex state by introducing an additional factor $R_{\rm s}$ for the dHvA oscillation amplitude:

$$R_{\rm s}=\exp\left(-\frac{\pi}{\omega_B\tau_{\rm s}}\right)=\exp\left(-\frac{2\pi^2k_{\rm B}T_\Delta}{\hbar\omega_B}\right), \qquad (38)$$

where the parameters $\tau_{\rm s}$ and T_Δ are directly connected with the extra Landau-level broadening $\Gamma_{\rm s}$ in the vortex state as $\Gamma_{\rm s}=\hbar/2\tau_{\rm s}=\pi k_{\rm B}T_\Delta$. The points with error bars in Fig. 8(b) shows $\ln R_{\rm s}$ as a function of $1/B$, i.e. the Dingle plot, obtained by numerical differentiation. This extra damping at high fields shows the behavior $\propto 1-B/H_{c2}$ in the logarithmic scale, but irregularity sets in around $0.55H_{c2}$ where the oscillation disappears. We attribute this irregularity to the effect of the bound-state formation in the core region.

The lines in Fig. 8(b) are the predictions from various theoretical formulas. Maki's formula[18] reproduces the correct functional behavior $\propto 1-B/H_{c2}$ at high fields, but the prefactor is seen too large. The NMA formula,[29] deduced from the two-dimensional self-consistent numerical results with $N_{\rm F}\sim 10$ at H_{c2}, predicts a more rapid attenuation incompatible with our numerical data. One reason for this discrepancy may originate from the fact that their numerical data with $N_{\rm F}\sim 10$ at H_{c2} are not appropriate for obtaining an analytic formula by fitting. Another may be attributed to the difference in dimensions. Indeed, the dHvA oscillation in three dimensions differs from that in two dimensions on the point that some finite region δp_z around the extremal orbit is relevant. Most of the Landau levels in the region do not satisfy the particle-hole symmetry with respect to $\varepsilon_{\rm F}$, so that the effect of the pair potential becomes smaller than that in two dimensions. Another theory by Dukan and Tešanović,[24] which would predict $R_{\rm s}=0$ in the clean limit of $T=0$, is also inconsistent with the data.

The red line in Fig. 8(b) is due to our formula for the extra Dingle temperature:

$$k_{\rm B}T_\Delta=0.5\tilde{\Gamma}\langle|\Delta_{\mathbf{p}}|^2\rangle_{\rm eo}\frac{m_{\rm b}c}{\pi e\hbar}\frac{1-B/H_{c2}}{B}, \qquad (39)$$

which is derived in Appendix C based on the second-order perturbation with respect to the pair potential. Here $\langle|\Delta_{\mathbf{p}}|^2\rangle_{\rm eo}$ denotes the average gap along the extremal or-

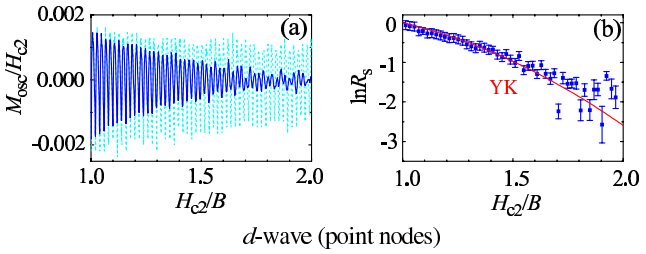

FIG. 10: (a) The oscillatory part of the magnetization $M_{\rm osc}$ in the vortex state (blue line) as compared with the normal-state one (sky-blue line) for the d-wave model of Eq. (32) at $T=0$. (b) The corresponding Dingle plot (points with error bars) as compared with the theoretical prediction (39).

bit at $B=0$, and $m_{\rm b}$ is the band mass. The numerical constant 0.5 stems from Eq. (36), and $\tilde{\Gamma}$ is a dimensionless quantity characterizing the Landau-level broadening due to the pair potential. This unknown parameter $\tilde{\Gamma}$ is determined by a best fit to the s-wave numerical data, i.e. the points with error bars in Fig. 8(b). This procedure yields

$$\tilde{\Gamma}=0.125\,.$$

We observe in Fig. 8(b) that Eq. (39), which predicts the dependence $\propto 1-B/H_{c2}$ for $\ln R_{\rm s}$, agrees with the numerical results. This formula will be seen below to reproduce other numerical data excellently without any adjustable parameters.

A difference of Eq. (39) from Maki's formula[18] lies in the prefactor where the Fermi velocity $v_{\rm F}$ is absent. Indeed, a dimensional analysis on the second-order perturbation tells us that the Landau-level broadening in the vortex state should be of order $|\tilde{\Delta}^{(0)}(B)|^2/\hbar\omega_B$, where $\tilde{\Delta}^{(0)}(B)\propto\sqrt{\langle|\Delta_{\mathbf{p}}|^2\rangle_{\rm eo}(1-B/H_{c2})}$ is essentially the average gap along the extremal orbit. This leads to Eq. (39) except for the numerical constant.

We now turn our attention to see how the presence of point nodes affect the dHvA oscillation. Figure 10(a) shows the oscillation of the d-wave magnetization (blue line) as compared with the normal-state one (sky-blue line). Although the d-wave gap in Eq. (32) has four point nodes on the Fermi surface along the extremal orbit, the damping is seen strong and not much different from the s-wave case. From this fact, we may conclude that it is the average gap along the extremal orbit which is relevant for the extra dHvA oscillation damping. Figure 10(b) presents the corresponding Dingle plot (points with error bars), which is compared with the prediction of Eq. (39). The formula with the average gap $\langle|\Delta_{\mathbf{p}}|^2\rangle_{\rm eo}$ reproduces the numerical result for $H_{c2}/B\lesssim 1.8$ excellently without adjustable parameters, thereby providing a strong support for the above statement.

This d-wave result is in disagreement with Miyake's theory that point nodes in the extremal orbit should weaken the attenuation.[19] Indeed, Miyake's theory is based on a semiclassical quantization for the expression

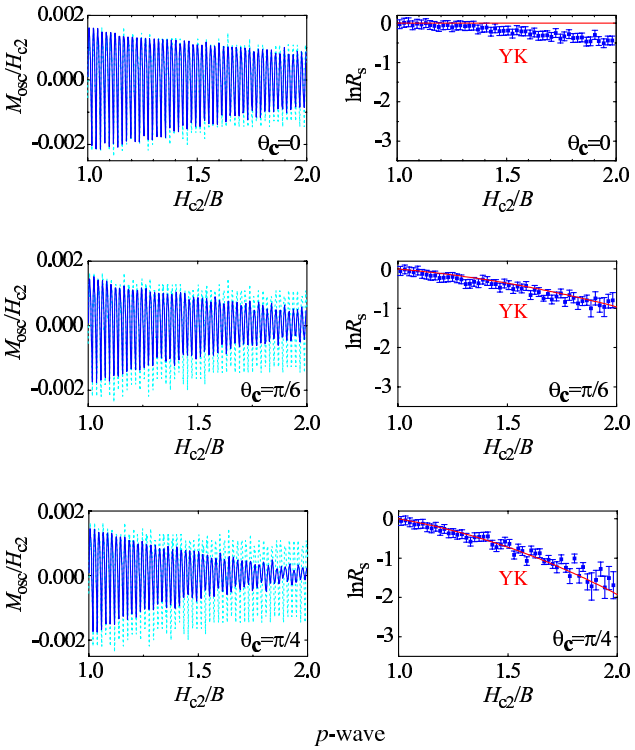

FIG. 11: Left figures: the oscillatory part of the magnetization $M_{\rm osc}$ in the vortex state (blue lines) as compared with the normal-state one (sky-blue lines) for the p-wave model of Eq. (32) at $T=0$. The crystal c axis, which is perpendicular to the nodal plane, is tilted from the field $\mathbf{B}$ by $\theta_{\mathbf{c}}=0$ (top), $\theta_{\mathbf{c}}=\pi/6$ (second), and $\theta_{\mathbf{c}}=\pi/4$ (bottom). Right figures: the corresponding Dingle plots (points with error bars) compared with Eq. (39).

of the electron number N_e at $B=0$. Neither his starting point $N_e(B=0)$ nor the use of the semiclassical quantization may be justified for describing the dHvA oscillation observed mainly near H_{c2}.

We finally consider the p-wave model with a line node in Eq. (32) to double-check the applicability of Eq. (39). The left figures in Fig. 11 display the dHvA oscillation for the line-node model, where the crystal c-axis is tilted from the magnetic-field direction by $\theta_{\mathbf{c}}=0$ (top), $\theta_{\mathbf{c}}=\pi/6$ (second), and $\theta_{\mathbf{c}}=\pi/4$ (bottom). The damping is seen weakest in the top figure where the gap vanishes along the extremal orbit, but increases gradually as finite gap opens along the orbit for $\theta_{\mathbf{c}}=0\to\pi/4$. These results indicate conclusively that the average gap along the extremal orbit is relevant for the extra dHvA attenuation. However, the non-zero extra damping in the top figure implies that not only the extremal orbit alone but some finite region around it contributes to the extra damping. Theoretically, this corresponds to the fact that we have to perform the Fresnel integral $\int_{-\infty}^{\infty}\exp[-i(\sqrt{2\pi N_{\rm F}}\,p_z/p_{\rm F})^2]\,dp_z$ for obtaining the LK formula in the normal state. Our data show that this off-extremal-orbit contribution cannot be neglected in the case where the gap vanishes exactly

TABLE I: Parameters characterizing three superconductors displaying the dHvA oscillation in the vortex state, together with values of the average gap along the extremal orbit $\sqrt{\langle|\Delta_{\rm p}|^2\rangle_{\rm eo}}$ estimated by Eq. (39). Here the symbol α and γ are band indices. These values of $\sqrt{\langle|\Delta_{\rm p}|^2\rangle_{\rm eo}}$ are to be compared with the band- and/or angle-averaged quantity $\Delta(0)$ extracted from a specific-heat experiment,[36] a far-infrared measurement,[51] a tunneling experiment,[52] or a Raman-scattering experiment.[53]

Compound	T_c (K)	$H_{c2}(T=0)$ (T)	$m_{\rm b}/m_e$	$\hbar\omega_{H_{c2}}$ (K)	$\hbar\omega_{H_{c2}}/k_{\rm B}T_c$	$\sqrt{\langle\|\Delta_{\rm p}\|^2\rangle_{\rm eo}}$ (meV)	$\Delta(0)$ (meV)
$NbSe_2$	7.2[16]	8.01 ($\theta=68.6^\circ$)[16]	0.61 (α)[16]	17.6[16]	2.20[16]	1.1 ($\pm$0.04)	1.1[51,52]
Nb_3Sn	18.3[7]	19.7 ($H\parallel c$)[7]	1.10 (γ)[7]	24.1[7]	1.31[7]	3.2 ($\pm$0.19)	3.2[53]
YNi_2B_2C	14.5[9]	8.8 ($H\parallel c$)[9]	0.35 (α)[9]	33.8[9]	2.33[9]	1.5 ($\pm$0.28)	2.5[36]

and completely at the extremal orbit. However, this off-extremal contribution is expected to become less important where finite gap is present along the extremal orbit. The right figures in Fig. 11 show the corresponding Dingle plot (points with error bars), which is compared with the prediction of Eq. (39). Except for the weak damping of $\theta_{\mathbf{c}}=0$ due to the off-extremal-orbit contribution, the formula is observed to reproduce the numerical results excellently.

V. ESTIMATION OF ENERGY GAP

Our calculations in Sec. IV C have clarified that (i) the gap anisotropy can be detected by measuring the extra dHvA oscillation damping in the vortex state, and (ii) Eq. (39) is particularly useful for this purpose. Using the formula, we finally provide quantitative estimations of the average gap along the extremal orbit for several materials displaying the dHvA oscillation in the vortex state. Table I summarizes parameters describing three relevant materials. These materials commonly have fairly high T_c's, and the ratio $\hbar\omega_{H_{c2}}/k_{\rm B}T_c$ ranges from 1 to 3. These features seem to be basic conditions for observing the dHvA oscillation in the vortex state. The values for $\sqrt{\langle|\Delta_{\rm p}|^2\rangle_{\rm eo}}$ are obtained by applying Eq. (39) to the observed dHvA attenuation in the vortex state. In doing so, we have adopted as m_b in Eq. (39) the values from dHvA experiments rather than those from band calculations, as indicated by the theory of Luttinger.[50] For comparison, we have also listed the values $\Delta(0)$ estimated by a specific-heat experiment,[36] a far-infrared measurement,[51] a tunneling experiment,[52] or a Raman-scattering experiment.[53] Thus, $\Delta(0)$ is expected to represent band- and/or angle-averaged energy gap. As seen in Table I, the two quantities coincide excellently for $NbSe_2$ and Nb_3Sn, indicating uniformly opened gap in these materials. On the other hand, $\sqrt{\langle|\Delta_{\rm p}|^2\rangle_{\rm eo}}=1.5$ for the α band of YNi_2B_2C is considerably smaller than $\Delta(0)=2.5$ from a specific-heat experiment.[36] This fact implies that YNi_2B_2C have large band- and/or angle-dependent gap anisotropy. Indeed, Bintley *et al.*[55] have recently carried out a detailed dHvA experiment on this material, rotating the field direction and observing the extra attenuation. They have reported a large angle dependence of the attenuation magnitude. They have also pointed out that their result is in agreement with the model with point nodes presented by Izawa *et al.*[37] based on a thermal-conductivity measurement.

VI. SUMMARY

We have carried out the first three-dimensional numerical calculations on the dHvA oscillation in the vortex state for various gap structures. We have thereby clarified the relation between gap anisotropy and persistence of the oscillation. We have also derived an analytic formula for the extra dHvA attenuation in the vortex state.

Our main results are given by Figs. 8-11 and Eq. (39). Those figures indicate clearly that the extra dHvA attenuation in the vortex state is directly connected with the average gap along the extremal orbit at $B=0$. The derived formula (39) have been shown to reproduce the numerical results excellently. Our theory attributes the origin of the extra dHvA damping to the Landau-level broadening caused by the pair potential. Hence the periodicity of the vortex lattice assumed here is almost irrelevant, and the theory is applicable also to the cases with irregularity such as a random array of vortices. Using Eq. (39), we have estimated average gap amplitudes along the extremal orbit for $NbSe_2$, Nb_3Sn, and YNi_2B_2C. The results indicate presence of large gap anisotropy in YNi_2B_2C.

Thus, we have shown explicitly that the dHvA effect in the vortex state can be a powerful tool to probe the average gap along the extremal orbit. Our results imply that, by rotating the field direction and observing the attenuation amplitude, we can obtain unique information on the band- and/or angle-dependent gap structure. Such an experiment has recently been performed on UPd_2Al_3 by Inada *et al.*[13] and on YNi_2B_2C by Bintley *et al.*,[55] and the latter group indeed has detected large gap anisotropy in the *ab* plane. Equation (39) will be useful in similar experiments for estimating band- and/or angle-dependent gap amplitudes.

Acknowledgments

We are grateful to F. J. Ohkawa for enlightening discussions. This research is supported by Grant-in-Aid for Scientific Research from the Ministry of Education, Culture, Sports, Science, and Technology of Japan.

APPENDIX A: THERMODYNAMIC POTENTIAL

The Luttinger-Ward thermodynamic potential corresponding to Eq. (1) is given by[56]

$$\Omega = -\frac{k_{\rm B}T}{2}\sum_n {\rm Tr}\ln\begin{bmatrix} \mathcal{H}-i\varepsilon_n & \Delta \\ \Delta^\dagger & -\mathcal{H}^*-i\varepsilon_n \end{bmatrix} \times \begin{bmatrix} {\rm e}^{i\varepsilon_n 0_+} & 0 \\ 0 & {\rm e}^{-i\varepsilon_n 0_+} \end{bmatrix} - \frac{1}{2}{\rm Tr}\,\Delta^\dagger\Phi\,, \tag{A1}$$

where we have adopted a compact notation of using $x\equiv \mathbf{r}\sigma$ with $\Delta_{\sigma_1\sigma_2}(\mathbf{r}_1,\mathbf{r}_2)\to\Delta(x_1,x_2)$, etc., and Tr also implies both integration and summation over $\mathbf{r}$ and σ, respectively. The quantity $\varepsilon_n/\hbar$ denotes the Matsubara frequency, and 0_+ is an infinitesimal positive constant. Now, Eq. (1) tells us that the first matrix in Eq. (A1) can be diagonalized as[56]

$$\begin{bmatrix} \mathcal{H}(x,x') & \Delta(x,x') \\ \Delta^\dagger(x,x') & -\mathcal{H}^*(x,x') \end{bmatrix} = \sum_s \begin{bmatrix} u_s^*(x) & -v_s(x) \\ v_s^*(x) & -u_s(x) \end{bmatrix}\begin{bmatrix} E_s & 0 \\ 0 & -E_s \end{bmatrix}\begin{bmatrix} u_s(x') & v_s(x') \\ -v_s^*(x') & -u_s^*(x') \end{bmatrix}. \tag{A2}$$

Substituting Eq. (A2) into Eq. (A1), the first term on the right-hand side becomes

$$-\frac{k_{\rm B}T}{2}\sum_{ns}\int {\rm d}x\,\big\{\big[|u_s(x)|^2{\rm e}^{z_n 0_+}+|v_s(x)|^2{\rm e}^{-z_n 0_+}\big] \times\ln(E_s-z_n) +\big[|v_s(x)|^2{\rm e}^{z_n 0_+}+|u_s(x)|^2{\rm e}^{-z_n 0_+}\big]\ln(-E_s-z_n)\big\}, \tag{A3}$$

with $z_n\equiv i\varepsilon_n$. The summation over n are then transformed with a standard technique[57] into a contour integral just above and below the real axis, using $f(z)\equiv({\rm e}^{z/k_{\rm B}T}+1)^{-1}$ and $f(-z)$ for the terms with ${\rm e}^{z_n 0_+}$ and ${\rm e}^{-z_n 0_+}$, respectively. Considering the poles inside the two contours and using $\int[|u_s(x)|^2+|v_s(x)|^2]{\rm d}x=1$, we obtain Eq. (6).

APPENDIX B: BASIS FUNCTIONS AND OVERLAP INTEGRALS

We here present explicit expressions for the quantities appearing in Eqs. (12) and (13); see Ref. 34 for their detailed derivations. It should be noted that we here adopt the symmetric gauge (3) which is more convenient than the Landau gauge used in Ref. 34. Hence there is an extra factor due to the gauge transformation in every expression of the basis functions, such as ${\rm e}^{-{\rm i}xy/2l_B^2}$ in Eq. (B1) below.

The basis function $\psi_{N\mathbf{k}\alpha}$ ($N=0,1,2,\cdots;\ \alpha=1,2$) in Eq. (12) is defined by

$$\psi_{N\mathbf{k}\alpha}(\mathbf{r}) = \sum_{n=-\mathcal{N}_{\rm f}/2+1}^{\mathcal{N}_{\rm f}/2} {\rm e}^{i[k_y(y+l_B^2k_x/2)+na_{1x}(y+l_B^2k_x-na_{1y}/2)/l_B^2]} \times{\rm e}^{-ixy/2l_B^2-(x-l_B^2k_y-na_{1x})^2/2l_B^2+i(\alpha-1)n\pi} \times\sqrt{\frac{a_{1x}/l_B}{2^N N!\sqrt{\pi}\,\mathcal{S}}}\,H_N\!\left(\frac{x-l_B^2k_y-na_{1x}}{l_B}\right), \tag{B1}$$

where $\mathcal{S}\equiv\pi l_B^2\mathcal{N}_{\rm f}^2$, and $H_N(x)\equiv{\rm e}^{x^2}\left(-\frac{\rm d}{{\rm d}x}\right)^N{\rm e}^{-x^2}$ is the Hermite polynomial.[58] The basis function $\psi^{(\rm c)}_{N\mathbf{q}}$ for the center-of-mass coordinates is obtained from Eq. (B1) by putting $\mathbf{k}\to\mathbf{q}$, $\alpha=1$, and $l_B\to l_{\rm c}\equiv l_B/\sqrt{2}$ as

$$\psi^{(\rm c)}_{N\mathbf{q}}(\mathbf{r}) = \sum_{n=-\mathcal{N}_{\rm f}/2+1}^{\mathcal{N}_{\rm f}/2} {\rm e}^{i[q_y(y+l_{\rm c}^2q_x/2)+na_{1x}(y+l_{\rm c}^2q_x-na_{1y}/2)/l_{\rm c}^2]} \times{\rm e}^{-ixy/2l_{\rm c}^2-(x-l_{\rm c}^2q_y-na_{1x})^2/2l_{\rm c}^2} \times\sqrt{\frac{a_{1x}/l_{\rm c}}{2^N N!\sqrt{\pi}\,\mathcal{S}}}\,H_N\!\left(\frac{x-l_{\rm c}^2q_y-na_{1x}}{l_{\rm c}}\right). \tag{B2}$$

Finally, the basis function ψ_{Nm} for the relative coordinates, which is conveniently chosen as an eigenstate of the orbital angular momentum operator $\hat{l}_z$, is given by

$$\psi^{(\rm r)}_{Nm}(\mathbf{r}) = \frac{(-1)^N}{\sqrt{2\pi}\,l_{\rm r}}\sqrt{\frac{N!}{(N+m)!}}\,\zeta^m\,{\rm e}^{-|\zeta|^2/2}\,L_N^{(m)}(|\zeta|^2)\,, \tag{B3}$$

where $\zeta\equiv(x+{\rm i}y)/\sqrt{2}l_{\rm r}$ with $l_{\rm r}\equiv\sqrt{2}l_B$, and $L_N^{(m)}(x)\equiv\frac{1}{N!}{\rm e}^x x^{-m}\left(\frac{\rm d}{{\rm d}x}\right)^N{\rm e}^{-x}x^{N+m}$ is the generalized Laguerre polynomial satisfying $N+m\geq 0$.[58]

We next provide expressions of the overlap integrals in Eq. (13). The first one, which was obtaind by Rajagopal and Ryan,[59] is given by

$$\langle N_{\rm c}N_{\rm r}|N_1N_2\rangle \equiv\delta_{N_1+N_2,N_{\rm c}+N_{\rm r}}\sqrt{\frac{N_1!N_2!N_{\rm c}!N_{\rm r}!}{2^{N_1+N_2}}} \times\sum_{n=\max(0,N_{\rm c}-N_2)}^{\min(N_1,N_{\rm c})}\frac{(-1)^{N_2-N_{\rm c}+n}}{n!\,(N_1-n)!\,(N_{\rm c}-n)!\,(N_2-N_{\rm c}+n)!}\,, \tag{B4}$$

which satisfies

$$\langle N_{\rm c}N_{\rm r}|N_1N_2\rangle = (-1)^{N_{\rm r}}\langle N_{\rm c}N_{\rm r}|N_2N_1\rangle\,, \tag{B5a}$$

$$\sum_{N_1N_2}\langle N'_{\rm c}N'_{\rm r}|N_1N_2\rangle\langle N_1N_2|N_{\rm c}N_{\rm r}\rangle = \delta_{N'_{\rm c}N_{\rm c}}\,\delta_{N'_{\rm r}N_{\rm r}}\,. \tag{B5b}$$

The asymptotic expression of Eq. (B4) for $N_{\rm c} \ll N_1, N_2$ is given by[34]

$$\langle N_{\rm c} N_{\rm r}|N_1 N_2\rangle \approx \delta_{N_1+N_2,N_{\rm c}+N_{\rm r}}\,(-1)^{N_2}\left[\frac{2}{\pi(N_{\rm c}+N_{\rm r})}\right]^{1/4} \times {\rm e}^{-x^2/2}\,\frac{H_{N_{\rm c}}(x)}{\sqrt{2^{N_{\rm c}}N_{\rm c}!}}\,, \tag{B6}$$

with $x \equiv (N_1-N_2)/\sqrt{2(N_{\rm c}+N_{\rm r})}$. This expression forms the basis for quasiclassical approximations.

The second overlap integral is given by

$$\langle \mathbf{q}|m+N_{\rm r}\rangle = \sqrt{2\pi}\,l_{\rm r}\,(-1)^{m+N_{\rm r}}\big[\psi^{\rm (r)}_{m+N_{\rm r}\mathbf{q}}(\mathbf{0})\big]^*\,, \tag{B7}$$

where $\psi^{\rm (r)}_{m+N_{\rm r}\mathbf{q}}$ is another basis function of the relative coordinates defined by

$$\psi^{\rm (r)}_{N\mathbf{q}}(\mathbf{r}) = \sum_{n=-\mathcal{N}_{\rm f}/4+1}^{\mathcal{N}_{\rm f}/4} {\rm e}^{i[q_y(y+l_{\rm r}^2 q_x/4)/2+2na_{1x}(y+l_{\rm r}^2 q_x/2-na_{1y})/l_{\rm r}^2]} \times {\rm e}^{-ixy/2l_{\rm r}^2-(x-l_{\rm r}^2 q_y/2-2na_{1x})^2/2l_{\rm r}^2} \times\sqrt{\frac{2a_{1x}/l_{\rm r}}{2^N N!\sqrt{\pi}\,\mathcal{S}}}\,H_N\!\left(\frac{x-l_{\rm r}^2 q_y/2-2na_{1x}}{l_{\rm r}}\right). \tag{B8}$$

APPENDIX C: ANALYTIC FORMULA FOR DHVA OSCILLATION DAMPING

In order to derive an analytic expression for the dHvA oscillation damping in the vortex states, we start from the thermodynamic potential of Eq. (6). The last term $-\frac{1}{2}{\rm Tr}\underline{\Delta}\,\underline{\Phi}$ may be expressed solely with respect to the pair potential, so that they can be neglected in the present model to consider the oscillatory part. Since we are interested in the extra damping in the vortex state, we adopt as E_s and $\mathbf{v}_s$ the expressions from the second-order perturbation with respect to $\underline{\Delta}$. They are obtained as

$$E_{N\mathbf{k}\alpha p_z\sigma} = |\xi_{Np_z\sigma}| + \eta^{(1)}_{N\mathbf{k}p_z}{\rm sign}(\xi_{Np_z\sigma})\,, \tag{C1}$$

$$\int|\mathbf{v}_{N\mathbf{k}\alpha p_z\sigma}(\mathbf{r})|^2 d\mathbf{r} = \theta(-\xi_{Np_z\sigma}) + \eta^{(2)}_{N\mathbf{k}p_z}{\rm sign}(\xi_{Np_z\sigma})\,, \tag{C2}$$

where θ is the step function, and $\eta^{(n)}_{N\mathbf{k}p_z}$ is defined by using Eq. (13a) as

$$\eta^{(n)}_{N\mathbf{k}p_z} \equiv \sum_{N'}\frac{|\Delta^{(\mathbf{k}p_z)}_{NN'}|^2}{(\xi_{Np_z}+\xi_{N'-p_z})^n}. \tag{C3}$$

The first terms on the right-hand side of Eqs. (C1) and (C2) are just the normal-state results. The second terms, on the other hand, denote the finite quasiparticle dispersion in the magnetic Brillouin zone and the smearing of the Fermi surface, respectively, due to the scattering by the growing pair potential. It is useful to express $\eta^{(n)}_{N\mathbf{k}p_z}$ in terms of $\tilde{\Delta}^{(0)}(B)$ and the cyclotron energy $\hbar\omega_B$ of the extremal orbit as

$$\eta^{(n)}_{N\mathbf{k}p_z} = \frac{|\tilde{\Delta}^{(0)}(B)|^2}{(\hbar\omega_B)^n}\,\tilde{\eta}^{(n)}_{N\mathbf{k}p_z}\,. \tag{C4}$$

The quantity $\tilde{\eta}^{(n)}_{N\mathbf{k}p_z}$ thus defined is dimensionless, and we realize that the main B dependence in Eq. (C4) lies in the prefactor $|\tilde{\Delta}^{(0)}(B)|^2/(\hbar\omega_B)^n$. The explicit expression of $\tilde{\eta}^{(n)}_{N\mathbf{k}p_z}$ is obtained by using Eqs. (13a) and (33). Considering the case $\theta_{\mathbf{c}}=0$, for simplicity, it is given by

$$\tilde{\eta}^{(n)}_{N\mathbf{k}p_z} = \frac{\mathcal{N}_{\rm f}^2}{4}\sum_{N'mm'}\frac{|\langle NN'|0\,N+N'\rangle|^2\langle N+N'+m|2\mathbf{k}-\mathbf{q}\rangle}{[N+N'-2(N_{\rm F}+\delta)]^n} \times\langle 2\mathbf{k}-\mathbf{q}|N+N'+m'\rangle\times\begin{cases}\delta_{m0}\delta_{m'0}\\ \delta_{m,\pm2}\delta_{m',\pm2}\sin^4\theta_{\mathbf{p}}\\ \delta_{m0}\delta_{m'0}\cos^2\theta_{\mathbf{p}}\end{cases}, \tag{C5}$$

where the quantity $\delta=\delta(B,p_z)$ ($|\delta|<1/2$) specifies the location of $\varepsilon_{\rm F}$ between the two closest Landau levels, and the overlap integrals are defined by Eqs. (B4) and (B7). The corresponding normalized density of states:

$$D^{(n)}_{Np_z}(\tilde{\eta}) \equiv \frac{2}{\mathcal{N}_{\rm f}^2}\sum_{\mathbf{k}\alpha}\delta(\,\tilde{\eta}-\tilde{\eta}^{(n)}_{N\mathbf{k}p_z}\,), \tag{C6}$$

will play a central role in the following.

Substituting Eqs. (C1) and (C2) into Eq. (6), we find that the terms containing $\eta^{(2)}_{N\mathbf{k}p_z}$ may be neglected due to the cancellation between the particle and hole contributions. The remaining term can be transformed with the standard procedure.[1] We thereby obtain, for the first harmonic of Ω/V, the expression:

$$\frac{\Omega_1}{V} = -\frac{k_{\rm B}T}{2\pi^2 l_B^2}\sum_\sigma\int_{-1/2}^{\infty}dN\cos(2\pi N)\int_{-\infty}^{\infty}dp_z\int_{-\infty}^{\infty}d\tilde{\eta} \times D^{(1)}_{Np_z}(\tilde{\eta})\ln\big[1+{\rm e}^{-(\xi_{Np_z\sigma}+\tilde{\eta}\,|\tilde{\Delta}^{(0)}(B)|^2/\hbar\omega_B)/k_{\rm B}T}\big]\,. \tag{C7}$$

The function $D^{(1)}_{Np_z}(\tilde{\eta})$ depends on (N,p_z), but may be replaced by a representative one $\overline{D}^{(1)}_\ell(\tilde{\eta})$ to be placed outside the N and p_z integrals,[60] where the recovered index ℓ specifies the s-, d-, or p-wave case of Eq. (C5). It may also be acceptable to use a Lorenzian for it: $\overline{D}^{(1)}_\ell(\tilde{\eta}) = \tilde{\Gamma}_\ell/\pi(\tilde{\eta}^2+\tilde{\Gamma}_\ell^2)$.[61] We thereby obtain an expression for the magnetization which carries an extra damping factor:

$$R_{\rm s}(B) \equiv \int_{-\infty}^{\infty}\overline{D}^{(1)}_\ell(\tilde{\eta})\exp\Big[-2\pi i\tilde{\eta}|\tilde{\Delta}^{(0)}(B)|^2/(\hbar\omega_B)^2\Big]\,d\tilde{\eta} = \exp\big[-2\pi\tilde{\Gamma}_\ell|\tilde{\Delta}^{(0)}(B)|^2/(\hbar\omega_B)^2\,\big]\,. \tag{C8}$$

Thus, the superconductivity gives rise to an extra Dingle temperature of $k_{\rm B}T_\Delta \equiv \tilde{\Gamma}_\ell\,|\tilde{\Delta}^{(0)}(B)|^2/\pi\hbar\omega_B$, or equivalently, the extra scattering rate of $\tau_{\rm s}^{-1} \equiv 2\pi k_{\rm B}T_\Delta/\hbar$.

Equation (C8) has an advantage that one can trace the origin of the extra dHvA damping definitely to the growing pair potential, which brings finite quasiparticle dispersion in the magnetic Brillouin zone as Eq. (C5), and the corresponding Landau-level broadening as Eq. (C6). Moreover, Eq. (C5) reveals that this broadening near H_{c2} is closely connected with the zero-field gap structure given by Eq. (32).

There seems to be no analytic way to estimate $\tilde{\Gamma}_s$, so we fix it through the best fit to the numerical data of Fig. 8(b). Using Eq. (34) with $a^2 = 0.5\Delta_0^2$, the procedure yields $\tilde{\Gamma}_s = 0.125$, as mentioned before. It is also clear both from Figs. 10 and 11 and from Eq. (C5) that the average gap around the extremal orbit is relevant for the extra attenuation. We hence put $a^2\tilde{\Gamma}_\ell = 0.5\langle|\Delta_{\mathbf{p}}|^2\rangle_{\rm eo}\tilde{\Gamma}_s$. We thereby obtain Eq. (39), which yields excellent fits to the d- and p-wave numerical data without any adjustable parameters, as seen in Figs. 10 and 11.

* URL: `http://phys.sci.hokudai.ac.jp/~kita/index-e.html`; Electronic address: kita@phys.sci.hokudai.ac.jp

1 I. M. Lifshitz and A. M. Kosevich: J. Exp. Theor. Phys. **29** (1955) 730 [Sov. Phys. JETP **2** (1956) 636].

2 D. Shoenberg: *Magnetic Oscillations in Metals* (Cambridge University Press, Cambridge, 1984).

3 J. E. Graebner and M. Robbins, Phys. Rev. Lett. **36**, 422 (1976).

4 Y. Ōnuki, I. Umehara, T. Ebihara, N. Nagai and K. Takita: J. Phys. Soc. Jpn. **61** (1992) 692.

5 F. M. Mueller, D. H. Lowndes, Y. K. Chang, A. J. Arko, and R. S. List, Phys. Rev. Lett. **68**, 3928 (1992).

6 R. Corcoran, N. Harrison, S. M. Hayden, P. Meeson, M. Springford, and P. J. van der Wel, Phys. Rev. Lett. **72**, 701 (1994).

7 N. Harrison, S. M. Hayden, P. Messon, M. Springford, P. J. van der Wel, and A. A. Menovsky: Phys. Rev. B**50**, 4208 (1994).

8 M. Heinecke and K. Winzer: Z. Phys. B**98**, 147 (1995); G. Goll, M. Heinecke, A. G. M. Jansen, W. Joss, L. Nguyen, E. Steep, K. Winzer and P. Wyder, Phys. Rev. B**53**, R8871 (1996).

9 T. Terashima, H. Takeya, S. Uji, K. Kadowaki and H. Aoki: Solid State Commun. **96**, 459 (1995); T. Terashima, C. Haworth, H. Takeya, S. Uji, H. Aoki, and K. Kadowaki, Phys. Rev. B**56**, 5120 (1997).

10 M. Hedo, Y. Inada, T. Ishida, E. Yamamoto, Y. Haga, Y. Ōnuki, M. Higuchi, and A. Hasegawa, J. Phys. Soc. Jpn. **64**, 4535 (1995).

11 H. Ohkuni, T. Ishida, Y. Inada, Y. Haga, E. Yamamoto, Y. Ōnuki, and S. Takahashi, J. Phys. Soc. Jpn. **66**, 945 (1997); H. Ohkuni, Y. Inada, Y. Tokiwa, K. Sakurai, R. Settai,T. Honma, Y. Haga, E. Yamamoto, Y. Ōnuki, H. Yamagami, S. Takahashi, and T. Yanagisawa, Phil. Mag. B**79**, 1045 (1999).

12 C. Bergemann, S. R. Julian, G. J. McMullan, B. K. Howard, G. G. Lonzarich, P. Lejay, J. P. Brison, and J. Flouquet, Physica B**230-232**, 348 (1997).

13 Y. Inada, H. Yamagami, Y. Haga, K. Sakurai, Y. Tokiwa, T. Honma, E. Yamamoto, Y. Ōnuki, and T. Yanagisawa, J. Phys. Soc. Jpn. **68**, 3643 (1999).

14 R. Settai, H. Shishido, S. Ikeda, Y. Murakawa, M. Nakashima, D. Aoki, Y. Haga, H. Harima, and Y. Ōnuki, J. Phys. Condens. Matter **13**, L627 (2001).

15 P. J. van der Wel, J. Caulfield, R. Corcoran, P. Day, S. M. Hayden, W. Hayes, M. Kurmoo, P. Meeson, J. Singleton, and M. Springford, Physica C**235-240**, 2453 (1994).

16 T. J. B. M. Janssen, C. Haworth, S. M. Hayden, P. Meeson, and M. Springford, Phys. Rev. B**57**, 11698 (1998).

17 Y. Inada and Y. Ōnuki, Fizika Nizkikh Temp. **25**, 775 (1999).

18 K. Maki, Phys. Rev. B**44**, 2861 (1991).

19 K. Miyake, Physica B**186-188**, 115 (1993).

20 L. P. Gor'kov and J. R. Schrieffer, Phys. Rev. Lett. **80**, 3360 (1998).

21 A. Wasserman and M. Springford, Physica B**194-196**, 1801 (1994).

22 M. J. Stephen, Phys. Rev. B**45**, 5481 (1992).

23 S. H. Curnoe, Phys. Rev. B**62**, 12413 (2000).

24 S. Dukan and Z. Tešanović, Phys. Rev. Lett. **74**, 2311 (1995).

25 T. Maniv, A. I. Rom, I. D. Vagner, and P. Wyder, Phys. Rev. B**46**, 8360 (1992).

26 M. G. Vavilov and V. P. Mineev, Zh. Exsp. Teor. Fiz. **112**, 1873 (1997) [Sov. Phys. JETP **85**, 1024 (1997]; V. P. Mineev, Phil. Mag. B**80**, 307 (2000).

27 G. M. Bruun, V. N. Nicopoulos, and N. F. Johnson, Phys. Rev. B**56**, 809 (1997).

28 V. M. Gvozdikov and M. V. Gvozdikova, Phys. Rev. B**58**, 8716 (1998).

29 M. R. Norman, A. H. MacDonald, and H. Akera, Phys. Rev. B**51**, 5927 (1995).

30 P. Miller and B. L. Györffy, J. Phys. Condens. Matter **7**, 5579 (1995).

31 U. Brandt, W. Pesch, and L. Tewordt, Z. Phys. **201**, 209 (1967).

32 R. B. Dingle, Proc. Roy. Soc. A**211**, 517 (1952).

33 This fact may be realized by observing that there is a clear zero-bias peak at the core (Fig. 8a) as well as the BCS gap structure (Fig. 8d) in their density of states. The sharp peaks in Fig. 8 may be due to a very small value of $p_{\rm F}\xi_0$ (~ 1) in their model.

34 T. Kita, J. Phys. Soc. Jpn. **67**, 2075 (1998).

35 K. Yasui and T. Kita, Phys. Rev. Lett. **86**, 1836 (1999).

36 R. Movshovich, M. F. Hundley, J. D. Thompson, P. C. Canfield, B. K. Cho and A. V. Chubukov: Physica C**227** (1994) 381.

37 K. Izawa, K. Kamata, Y. Nakajima, Y. Matsuda, T. Watanabe, M. Nohara, H. Takagi, P. Thalmeier, and K. Maki, cond-mat/0205178.

38 K. Yasui and T. Kita: J. Phys. Soc. Jpn. **70**, 2852 (2001).

39 T. Kita, J. Phys. Soc. Jpn. **67**, 2067 (1998).

40 See, e.g., L. I. Schiff: *quantum mechanics* 3rd ed. (McGraw-Hill, New York, 1981).

[41] J. C. Ryan and A. K. Rajagopal: Phys. Rev. B**47** (1993) 8843.
[42] E. Helfand and N. R. Werthamer: Phys. Rev. **147** (1966) 288.
[43] H. Won and K. Maki, Phys. Rev. B**53**, 5927 (1996).
[44] M. Ichioka, A. Hasegawa, and K. Machida, Phys. Rev. B**59**, 8902 (1999).
[45] R. Gilardi, J. Mesot, A. Drew, U. Divakar, S. L. Lee, E. M. Forgan, O. Zaharko, K. Conder, V. K. Aswal, C. D. Dewhurst, R. Cubitt, N. Momono, and M. Oda, Phys. Rev. Lett. **88**, 217003 (2002).
[46] M. Rasolt, Phys. Rev. Lett. **58**, 1482 (1987).
[47] A. H. MacDonald, H. Akera, and M. R. Norman, Phys. Rev. B**45**, 10147 (1992).
[48] For a review on this topic, see, M. Rasolt and Z. Tešanović, Rev. Mod. Phys. **64**, 709 (1992).
[49] M. Franz and Z. Tešanović, Phys. Rev. Lett. **80**, 4763 (1998).
[50] J. M. Luttinger, Phys. Rev. **121**, 1251 (1961).
[51] B. P. Clayman and R. F. Frindt, Solid State Commun. **9**, 1881 (1971).
[52] D. H. Lee, L. W. Dubeck, and F. Rothwarf, Phys. Lett. **53A**, 379 (1975).
[53] R. Hackl, R. Kaiser, and S. Schicktanz, J. Phys. C **16**, 1729 (1983).
[54] J. C. F. Brock, Solid State Commun. **7**, 1789 (1969).
[55] D. Bintley and P. J. Meeson, unpublished.
[56] T. Kita: J. Phys. Soc. Jpn. **65** (1996) 1355.
[57] J. M. Luttinger and J. C. Ward, Phys. Rev. **118**, 1417 (1960).
[58] See, e.g., M. Abramowitz and I. A. Stegun: *Handbook of Mathematical Functions* 10th ed. (Dover, New York, 1972).
[59] A. K. Rajagopal and J. C. Ryan: Phys. Rev. B**44** (1991) 10280.
[60] The p_z integral in Eq. (C7) passes through regions where $\delta \approx 0$ in Eq. (C5), i.e., the second-order perturbation is not justified. However, the main contribution to the integral certainly comes from the regions where we can use Eq. (C1). Notice that $\delta = -1/8$ at the maximal orbit when the magnetization takes a local maximum.
[61] It is found numerically that the variance of Eq. (C6) depends little on the values of $N_{\rm F}$ and N ($\sim N_{\rm F}$), as expected. It is ~ 0.2 for the s-wave pairing with $\delta = -1/8$.